Journal of
Medicinal Chemistry

Article

Optimizing the Benefit/Risk of Acetyl-CoA Carboxylase (ACC) Inhibitors Through Liver Targeting

Kim Huard, Aaron C. Smith, Gregg D Cappon, Robert L. Dow, David J. Edmonds, Ayman El-Kattan, William P Esler, Dilinie P. Fernando, David A. Griffith, Amit S. Kalgutkar, Trenton Ross, Scott W. Bagley, David Beebe, Yi-An Bi, Shawn Cabral, Collin Crowley, Shawn D Doran, Matthew S. Dowling, Spiros Liras, Vincent Mascitti, Mark Niosi, Jeffrey A. Pfefferkorn, Jana Polivkova, Cathy Preville, David A. Price, Andre Shavnya, Norimitsu Shirai, Andrew H Smith, James A Southers, David A Tess, Benjamin A. Thuma, Manthena V. S. Varma, and Xiaojing Helen Yang

J. Med. Chem., **Just Accepted Manuscript** • DOI: 10.1021/acs.jmedchem.0c00640 • Publication Date (Web): 18 Aug 2020

Just Accepted

is published by the American Chemical Society. 1155 Sixteenth Street N.W., Washington, DC 20036

Optimizing the Benefit/Risk of Acetyl-CoA Carboxylase (ACC) Inhibitors Through Liver Targeting

Kim Huard,[◊] Aaron C. Smith,[†] Gregg Cappon,[†] Robert L. Dow,[◊] David J. Edmonds,[◊] Ayman El-Kattan,[◊] William P. Esler,[◊] Dilinie P. Fernando,[†] David A. Griffith,[◊] Amit S. Kalgutkar,[◊] Trenton T. Ross,[◊] Scott W. Bagley,[†] David Beebe,[◊] Yi-An Bi,[†] Shawn Cabral,[†] Collin Crowley,[◊] Shawn D. Doran,[†] Matthew S. Dowling,[†] Spiros Liras,[◊] Vincent Mascitti,[†] Mark Niosi,[†] Jeffrey A. Pfefferkorn,[◊] Jana Polivkova,[†] Cathy Préville,[†] David A. Price,[◊] Andre Shavnya,[†] Norimitsu Shirai,[†] Andrew H. Smith,[†] James R. Southers,[†] David A. Tess,[◊] Benjamin A. Thuma,[†] Manthena V. Varma,[†] Xiaojing Yang[†]*

[◊]Pfizer Worldwide Research and Development, 1 Portland Street, Cambridge, Massachusetts USA 02139

[†]Pfizer Worldwide Research and Development, Eastern Point Road, Groton, Connecticut USA 06340

KEYWORDS: Hepatoselective, liver targeting, acetyl CoA carboxylase, inhibitor, organic anion transporting peptide, CYP, NAFLD, NASH, DNL, PF-05221304.

ABSTRACT: Preclinical and clinical data suggest that acetyl-CoA carboxylase (ACC) inhibitors have the potential to rebalance disordered lipid metabolism leading to improvements in non-alcoholic steatohepatitis (NASH). Consistent with these observations, first-in-human clinical trials with our ACC inhibitor PF-05175157 led to robust reduction of de novo lipogenesis (DNL), albeit with concomitant reductions in platelet count, which were attributed to the inhibition of fatty acid synthesis within bone marrow. Herein we describe the design, synthesis, and evaluation of carboxylic acid-based ACC inhibitors with organic anion transporting polypeptide (OATP) substrate properties, which facilitated selective distribution of the compounds at the therapeutic site of action (liver) relative to the periphery. These efforts led to the discovery of clinical candidate PF-05221304 (**12**), which selectively inhibits liver DNL in animals, while demonstrating considerable safety margins against platelet reduction in a non-human primate model.

INTRODUCTION

Acetyl-CoA carboxylase (ACC) is a key enzyme regulating lipid metabolism.[1] There are two closely related isoforms of ACC that differ in tissue distribution: ACC1 is more highly expressed in lipogenic tissues such as liver and adipose, while ACC2 is the major isoform expressed in oxidative tissues such as skeletal and heart muscle. ACC catalyzes the ATP-dependent condensation of acetyl-CoA with carbonate to produce malonyl-CoA, which is a rate-limiting substrate for de novo lipogenesis (DNL). In addition, malonyl-CoA acts as an allosteric inhibitor of the enzyme carnitine palmitoyltransferase 1, which is responsible for catalyzing the rate limiting transport of medium and long chain fatty acyl-CoAs into the mitochondria for fatty acid oxidation. Hence, through the intermediacy of malonyl-CoA, ACC serves as a critical switch regulating the transition from lipogenic to oxidative lipid metabolism.

Identification of small molecule inhibitors of ACC has been of long-standing interest for treating multiple indications including type 2 diabetes mellitus (T2DM), non-alcoholic fatty liver disease (NAFLD) and aspects of the metabolic syndrome,[2-6] oncology,[7, 8] and acne vulgarus.[9] Pfizer efforts towards ACC inhibitors identified screening hit CP-610431 (**1**),[2] which was optimized to provide pre-candidate **2**[10-12] and first generation clinical candidate PF-05175157 (**3**),[13] both dual ACC1 and ACC2 inhibitors (Figure 1).

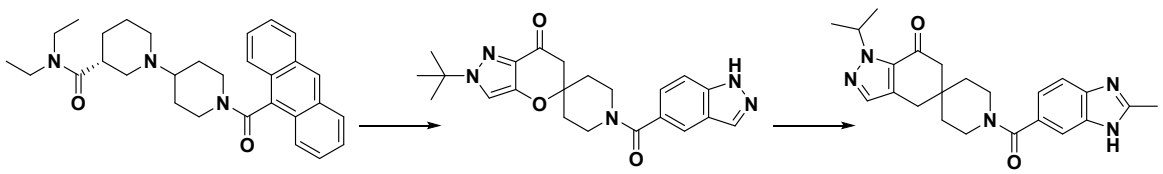

Figure 1. Systemic ACC inhibitors identified from the Pfizer program

Compound **3** inhibited hepatic DNL and lowered the respiratory exchange ratio in healthy human volunteers.[9, 13] These observations indicated that the inhibition of ACC1 and ACC2 in humans increases dependence on whole-body fatty acid utilization. While **3** was generally well-tolerated in human clinical studies, development was terminated due to asymptomatic reductions in platelet count observed during multi-dose studies in human volunteers with type 2 diabetic mellitus.[14] Platelet count reductions had not been observed in the regulatory toxicology studies in rats and dogs which supported the conduct of human clinical trials. However, we subsequently found that ACC inhibition reduces platelet count in nonhuman primates (NHPs).[14] Since this model verified the clinical results observed with **3**, it would be useful for predicting the platelet lowering effects of other ACC inhibitors in humans.[14] A combination of ex vivo assays and in vivo toxicology assessments in NHPs demonstrated that reductions in platelet count were secondary to ACC inhibition within bone marrow, which prevented the normal formation of platelets due to attenuation of bone marrow DNL and subsequent impairment of megakaryocyte maturation.[14]

Recently, there is growing interest in using ACC inhibitors for the treatment of NAFLD and non-alcoholic steatohepatitis (NASH).[15, 16] NASH is a clinical and histological subset of NAFLD that is associated with increased all-cause mortality, cirrhosis and end-stage liver disease, increased cardiovascular mortality, and increased incidence of both liver related and non-liver related cancers.[17] In the US population, the prevalence of NAFLD and NASH is estimated at 30–40% and 3–5%, respectively.[18]

Alterations in lipid metabolism are hypothesized to contribute to the molecular pathogenesis of NAFLD and NASH. Human subjects with elevated levels of liver fat have more than a three-fold higher rate of hepatic DNL relative to subjects with normal amounts of liver fat.[19] ACC

inhibitors have the potential to alter the balance of hepatic TG accumulation and modulation of fat production and/or clearance, and this is expected to reduce both liver fat and steatosis in patients with NASH. In rats, ACC inhibition stimulates fatty acid oxidation, suppresses hepatic DNL, and consequently reduces steatosis.[20, 21] Improvements in steatosis were also observed in human subjects treated with ACC inhibitors.[3, 4, 6, 22, 23] Furthermore, amelioration of steatosis is hypothesized to suppress hepatic inflammation and subsequently reduce fibrogenesis.[24] While the ACC inhibitors MK-4074[4] and GS-0976[3, 5, 6, 22, 23] (Figure 2) have been studied in clinical trials for the treatment of NASH/NAFLD, there are currently no approved therapies for the treatment of this disease, resulting in a significant unmet medical need.

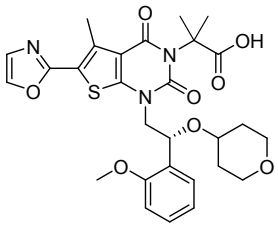

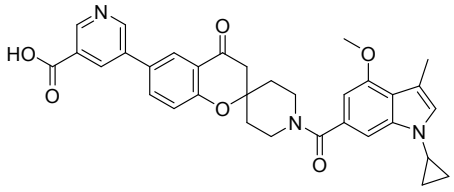

Figure 2. Liver-targeted ACC inhibitors in clinical development

Although ACC inhibitors have the potential to address multiple pathogenic contributors to NASH, the importance of DNL within human bone marrow for platelet production limits the degree of systemic ACC inhibition safely tolerated during chronic treatment.[14] We hypothesized that an ACC inhibitor with asymmetric tissue distribution favoring the liver, the site of action for intervention in NASH, would have an improved therapeutic index for platelet lowering relative to compound **3** by minimizing ACC inhibition in bone marrow. To test this hypothesis, we undertook the design, synthesis, and evaluation of ACC inhibitors with the incorporation of structural features intended for recognition by organic anion transporting polypeptides (OATPs),

members of the SCLO superfamily of xenobiotic transporters.[25] Of the 11 human OATP transporters, OATP1B1 and OATP1B3 are expressed on the sinusoidal membrane of hepatocytes and can facilitate the liver uptake of their respective substrates (e.g., statins such as atorvastatin and rosuvastatin).[26] Consequently, we sought ACC inhibitors that were OATP1B1/1B3 transport substrates to drive hepatoselectivity.[17-21] Active transport to the liver by OATPs not only influences tissue distribution but also serves as a clearance mechanism of its substrates.[27] Hence, ensuring that the hepatoselective nature of the ACC inhibitors did not interfere with the otherwise attractive preclinical (and clinical) pharmacokinetics and disposition attributes observed with **3** was an important consideration in the design elements of our program. Herein, we describe the design and evaluation of clinical candidate PF-05221304 (**12**),[28] a liver-targeted dual ACC1 and ACC2 inhibitor. The OATP substrate properties of **12** result in pronounced asymmetrical tissue distribution of **12** in preclinical species. Consistent with its hepatoselectivity, **12** selectively inhibited DNL in the liver relative to bone marrow in rats and had an improved safety profile for effects on platelet count in NHPs relative to **3**. It is interesting to note that the carboxylic acid-containing ACC inhibitors GS-0976[3, 5, 6, 22, 23] and MK-4074[4] (Figure 2) have also been reported to be OATP substrates, but detailed structure-activity relationship analysis leading to their identification has not been published.

RESULTS AND DISCUSSION

Optimization of Acidic ACC Inhibitors. Since OATP substrates are anionic in nature (e.g., carboxylates)[29-32] with a relatively high molecular weight (MW $\geq$ 400 Da),[29, 33] our approach to the development of hepatoselective ACC inhibitors began with structural modifications of the potent systemic inhibitors **2** and **3** to include a carboxylic acid. Initial studies focused on probing vectors most likely to retain potency against ACC while bearing such a polar and ionizable

functional group. The x-ray co-crystal structure of compound **2** bound to ACC suggested limited opportunities to append a carboxylic acid within the central spirocyclic core, however there was a likelihood that acidic motifs could be tolerated at either end of the structure.[13] To this end, a set of carboxylic acid-containing analogs was prepared and a selection of analogs and their in vitro ACC inhibitory activity is reported in Table 1. As illustrated with compound **4**, direct functionalization of neutral analogs with a carboxylic acid on the pyrazole caused a significant decrease in potency against both ACC isoforms, and also led to a decrease in passive permeability (P_{app}) in Madin-Darby kidney cell line-low efflux (MDCK-LE) cells. On the other hand, substitution of the 6,5-fused heteroaryl at the distal end had modest impacts on potency as illustrated by indazole **5**. Unfortunately, the x-ray co-crystal structure of **2** bound to a humanized yeast chimeric carboxyltransferase domain of ACC was poorly resolved in the distal region, preventing the use of structure-based drug design to optimize the placement of the carboxylic acid or other anionic substituents in order to improve potency. Transforming the 6,5-fused heteroaryl moiety into an unfused biaryl offered more design opportunities to locate an optimal position for placement of a carboxylic acid while seeking to improve potency. Substitution of the carboxylic acid on the terminal phenyl ring (compounds **6** and **7**) was then carried out. The para-substituted carboxylic acid (**6**) had the greatest potency of the tested ideas but was relatively modest in comparison to **3**.[13]

Table 1. In vitro inhibitory potency against ACC1 and ACC2 and passive permeability of carboxylic acid-containing analogs

Compound	Structure	ACC1 $IC_{50}{}^{a}$ (μM)	ACC2 $IC_{50}{}^{a}$ (μM)	$P_{app}{}^{c}$ (10^{-6} cm/s)

2[13]	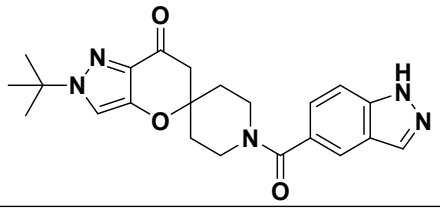	0.111 (7.0 ± 0.2)	0.0098 (8.0 ± 0.2)	13
3[13]	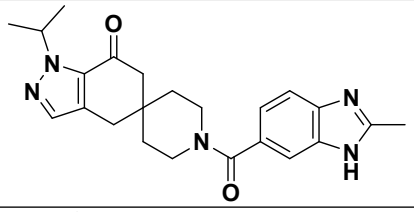	0.098 (7.0 ± 0.4)	0.045 (7.3 ± 0.5)	9.5
4	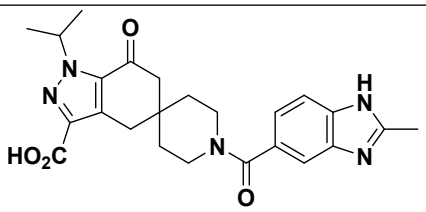	12 (4.9 ± 0.1)	1.2 (5.9 ± 0.3)	0.5
5	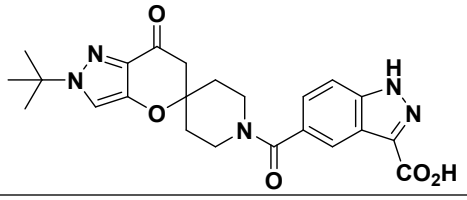	0.13 (6.9 ± 0.2)	0.033 (7.5 ± 0.1)	<0.4
6	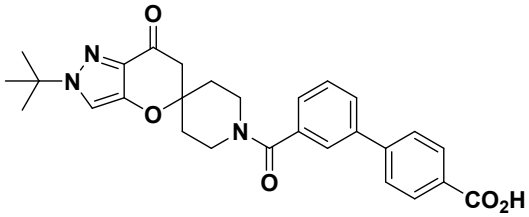	0.44 (6.4 ± 0.1)	0.092 (7.0 ± 0.2)	2.5
7	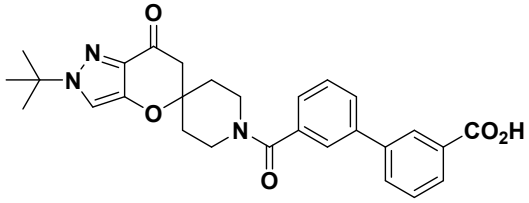	1.5 (5.8 ± 0.2)	0.20 (6.7 ± 0.2)	1.3

[a]In vitro potency against human recombinant ACC1 and ACC2 was determined using a Transcreener® assay as previously described.[10] IC_{50} values are reported as geometric mean of at least three replicates with pIC_{50} ± SD in parentheses. [c]Apparent passive permeability was assessed in Madin-Darby canine kidney cell line-low efflux cells with a 30 min pre-incubation time.[34] ND = not determined.

Acid **6** was further optimized to boost potency and new analogs were evaluated in vitro for lipophilicity (logD at pH 7.4 using the shake-flask method),[35] P_{app} in the MDCK-LE cellular assay,[34] with a 30 min pre-incubation time, and metabolic intrinsic clearance ($CL_{int,met}$) in human

hepatocytes (HHEPs).[36] Data on a focused set of analogs derived from the most potent biaryl isomer, compound **6**, is presented in Table 2. The phenyl ring proximal to the core of **6** was modified using parallel medicinal chemistry which led to the identification of **8** with considerable improvements in ACC inhibitory potency and low metabolic turnover ($CL_{int,met}$ < 3.0 μL/min/10^6 cells) in HHEPs.[36] Deletion of the methoxy group (**9**) led to a large drop off in ACC inhibitory potency. Replacement of the methoxy group in **8** with a *N*,*N*-dimethylamino substituent (compound **10**) maintained inhibitory potency, however $CL_{int,met}$ increased. Furthermore, passive permeability decreased in the MDCK-LE assay, potentially hindering oral (PO) absorption in pharmacokinetic studies. Given the good potency and metabolic clearance of **8**, its human OATP1B1 and OATP1B3 substrate properties were assessed using a differential uptake format in human embryonic kidney (HEK)293 cells transfected with the relevant transporter.[37] A normalized OATP1B1- and OATP1B3-mediated uptake ratio of > 2.0,[38] calculated as the total uptake of compound **8** in OATP-expressing cells divided by uptake observed in non-transfected parental cells, was observed suggesting that it was an OATP substrate with the potential to be hepatoselective.

Table 2. In vitro inhibitory potency against ACC1 and ACC2, lipophilicity (logD), metabolic intrinsic clearance, passive permeability, and OATP uptake ratios of analogs derived from compound **6**

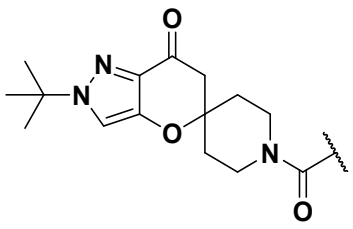

Compound	Structure	ACC1 IC_{50}[a] (μM)	ACC2 IC_{50}[a] (μM)	logD[b]	P_{app}[c] (10^{-6} cm/s)	HHEP $CL_{int,met}$[d] (μL/min/10^6)	HEK-OATP1B1 Uptake Ratio[e]	HEK-OATP1B3 Uptake Ratio[e]
8	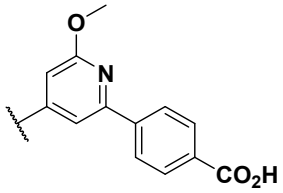	0.022 (7.7 ± 0.2)	0.013 (7.9 ± 0.4)	0.5	2.0	<3.0	5.0	3.3
9	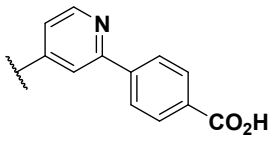	1.1 (6.0 ± 0.1)	0.19 (6.7 ± 0.1)	–0.4	ND	ND	ND	ND
10	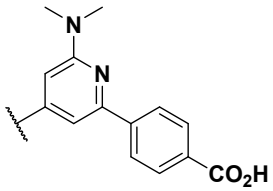	0.017 (7.8 ± 0.2)	0.0094 (8.0 ± 0.2)	0.8	0.5[f]	7.5	ND	ND

[a]In vitro potency against ACC1 and ACC2 was determined using a Transcreener® assay as previously described.[10] IC_{50} values are reported as geometric mean of at least three replicates with pIC_{50} ± SD in parentheses. [b]logD values were determined using the shake-flask method with an octanol/water partition at pH 7.4.[35] [c]Apparent permeability was assessed in MDCK-LE cells with a 30 min pre-incubation time.[34] [d]Metabolic intrinsic clearance obtained from scaling in vitro half-lives in cryopreserved human hepatocyte incubations conducted for 2 h as previously described.[36] [e]Ratio of total/passive cellular uptake as measured by compound uptake in OATP-transfected and parental cells for 5 min at 37 °C, respectively at a dose of 1 μM.[37] A ratio > 2 indicates the compound is a substrate in vitro.[38] [f]No pre-incubation was performed. ND = not determined.

To this point, the structure activity relationship for this series had been mostly developed with the N-2 *t*-butyl pyrazole spirocyclic ether found in compound **2**. Previous experience from the development of **3**[13] indicated that permeability could be improved by moving the pyrazole substituent to the N-1 position as found in compound **3** (data not shown), likely due to steric shielding of the ketone carbonyl group that increases lipophilicity. Additionally, changing from the cyclic ether to the carbocycle obviates the potential for retro-Michael ring-opening.[13]

Combining the N-1 *i*-propyl pyrazole spirocycle with optimized *N*,*N*-dimethylamino- and methoxy-substituted biaryl acids led to potent analogs **11** and **12** with increased lipophilicity. This effectively translated to improved passive cell permeability without affecting metabolic stability (Table 3). Additionally, OATP uptake ratios were sufficiently high to suggest that **11** and **12** were substrates for hepatic transporters.

Table 3. In vitro inhibitory potency against ACC1 and ACC2, lipophilicity, metabolic intrinsic clearance, passive permeability, and OATP uptake ratios of optimized analogs

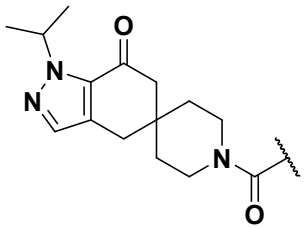

Compound	Structure	ACC1 IC_{50}[a] (μM)	ACC2 IC_{50}[a] (μM)	logD[b]	P_{app}[c] (10^{-6} cm/s)	HHEP $CL_{int,met}$[d] (μL/min/10^6)	HEK-OATP1B1 Uptake Ratio[e]	HEK-OATP1B3 Uptake Ratio[e]
11	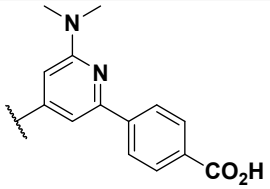	0.0077 (8.1 ± 0.3)	0.0056 (8.3 ± 0.2)	1.4	13	<3.0	2.1	1.4
12	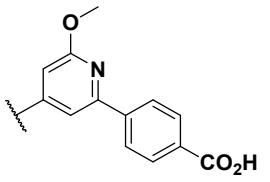	0.033 (7.5 ± 0.1)	0.026 (7.6 ± 0.2)	1.1	14	<3.0	3.5	2.5

[a]In vitro potency against ACC1 and ACC2 was determined using a Transcreener® assay as previously described.[10] IC_{50} values are reported as geometric mean of at least three replicates with pIC_{50} ± SD in parentheses. [b]logD values were determined using the shake-flask method with an octanol/water partition at pH 7.4.[35] [c]Apparent permeability was assessed in MDCK-LE cells with a 30 min pre-incubation time.[34] [d]Metabolic intrinsic clearance obtained from scaling in vitro half-lives in cryopreserved human hepatocyte incubations conducted for 2 h as previously

described.[36] [e]Ratio of total/passive cellular uptake as measured in OATP-transfected and parental cells, respectively at doses of 1–3 μM at 0.5–4.0 min.[37] A ratio > 2 indicates the compound is a substrate in vitro.[38]

Evaluation of In Vivo Hepatoselectivity in Rats. To confirm the in vitro observations of OATP-mediated uptake in an in vivo setting, compounds **8**, **11**, and **12** were administered via PO gavage to rats and unbound liver-to-plasma concentration ratios ($K_{pu,u}$) were determined 6 h post-dose. Total K_p values greater than unity and $K_{pu,u}$ values ranging from 79 to 376 were observed for **8**, **11**, and **12** (Table 4), which is consistent with selective distribution of the three compounds in the liver most likely via hepatic uptake mediated by rat Oatp isoforms.

Table 4. Determination of unbound liver-to-plasma ratios ($K_{pu,u}$) for **8**, **11**, and **12** in animals

Compound	Species	$f_{u,plasma}$[a]	$f_{u,liver}$[a]	Dose (mg/kg)	Mean total concentration (ng/mL)[c]		K_p[d]	$K_{pu,u}$[e]
					Plasma	Liver		
8	Rat	0.17	0.07	30[b]	41.7	38100	914	376
11	Rat	0.057	0.026	10[b,f]	57.4	9920	173	79
12	Rat	0.0392	0.066	10[b]	314	24600	78	132
12	NHP	0.00956	0.15	1[g]	88	1300	15	230

All procedures performed on rats and monkeys were in accordance with regulations and established guidelines and were reviewed and approved by Pfizer Institutional Animal Care and Use Committee (IACUC).

[a]Fraction unbound (f_u) in plasma and liver tissue was determined by equilibrium dialysis.[39] [b]Compounds **8**, **11**, and **12** were administered as PO suspensions in 0.5% methyl cellulose containing 0.1% Tween 80 to male Wistar-Hannover rats (n = 2 or 3 animals). [c]Total concentrations in plasma and liver tissue were obtained 6 h post-dose and were converted into unbound values by multiplying with the corresponding f_u values in plasma or liver tissue. [d] K_p refers to the ratio of total liver concentrations divided by total plasma concentrations. [e]Unbound liver-to-plasma ratio ($K_{pu,u}$) was determined as the ratio of mean free liver to plasma concentrations. [f]**11** was administered as a hydrochloride salt. [g]**12** was administered intravenously (IV) as a tris(hydroxymethyl)aminomethane (tris) salt in a solution of 2% N-methylpyrrolidone and 98% sulfobutylether-betacyclodextrin (12.5%) in 50 mM TRIS buffer, pH 8.0 (n = 2).

Encouraged by the level of liver selectivity observed, the pharmacokinetic profiles of **8**, **11**, and **12** were examined in rats (Table 5). Relative to compounds **8** and **11**, **12** demonstrated a considerably lower plasma clearance (CL_p) and a longer terminal half-life ($t_{1/2}$) upon IV administration to rats. Moreover, IV administration of **12** to NHPs also led to a very low CL_p rate and a low steady state distribution volume (V_{ss}), which translated in a long terminal half-life ($t_{1/2}$) of ~ 11 h (see Table 5). PO pharmacokinetics studies in rats with the crystalline free form of **8** and **11** revealed that both compounds suffered from low oral bioavailability (F). In the case of **8**, the oral F of ~ 27% was commensurate with its high CL_p (54 mL/min/kg) in rats. In contrast, **11** demonstrated a lower CL_p relative to **8** in rats but was not systemically exposed when administered orally. Poor PO exposure (assessed by the maximal plasma concentrations (C_{max}) and area under the plasma concentration-time curve (AUC)) possibly reflected solubility-limited absorption (in addition to first-pass hepatic uptake/metabolism processes leading to the observed CL_p of 31 mL/min/kg) since **11** suffered from low thermodynamic aqueous solubility (pH 1.2 (2.0 μM), 6.5 (3.0 μM), and 7.4 (13 μM)). Although, the free form of crystalline **12** was more soluble (pH 1.2 (8.0 μM), 6.5 (36.0 μM), and 7.4 (234 μM)) than **11**, PO pharmacokinetic studies with **12** were conducted with the corresponding tris(hydroxymethyl)aminomethane (tris) salt form, which had improved aqueous solubility (pH 1.2 (1324 μM), 6.5 (3981 μM), and 7.4 (4772 μM)) over the free acid form. As shown in Table 5, PO administration of the tris salt of **12** led to rapid absorption (time to reach C_{max} (T_{max}) ~ 0.5–1.1 h) in rats and NHPs with oral F values of 48% and 50%, respectively. The corresponding fraction of the oral dose absorbed[40] was estimated to be 78% (rats) and 55% (NHPs).

Compound **12** demonstrated negligible renal excretion (< 2% of administered dose) as unchanged parent in rats upon IV dosing and lack of renal clearance was also noted in the IV

pharmacokinetic study in NHPs. The potential of **12** to undergo biliary elimination in unchanged form was also examined in rats. Approximately 12% of the administered IV dose (1 mg/kg) was recovered in unchanged form in pooled (0–24 h) rat bile, implying that biliary elimination of **12** was minimal in this species. Moreover, IV administration (1 mg/kg) of **12** to NHPs resulted in a mean $K_{pu,u}$ value of 166 (Table 4) six hours post-dose, which provided further proof of its hepatoselective properties mediated through OATP transporters. Given the good balance of ACC inhibitory potency, desirable preclinical tissue distribution on a compound with high permeability, and good pharmacokinetics, **12** was selected for further evaluation.

Table 5. Preclinical pharmacokinetics of **8**, **11**, and **12**[a]

Compound	Species	Route/ Dose (mg/kg)	CL_p (mL/min/kg)	V_{ss} (L/kg)	$t_{1/2}$ (h)	C_{max} (ng/mL)	T_{max} (h)	$AUC_{(0-24)}$ (ng.h/mL)	Oral F (%)
8	Rat	IV/1[b]	54.5	4.1	3.5	NA	NA	299	
		PO/4	NA	NA	5.7	53.9	0.75	322	27
11	Rat	IV/1[b]	31.3	5.2	7.5	NA	NA	519	
		PO/4	NA	NA	NA	–[f]	NA	–[f]	ND
12	Rat	IV/1[c]	16	7.2	8.6	NA	NA	965	
		PO/5[d]	NA	NA	5.6	390	0.54	2490	48
	NHP	IV/1[e]	1.3	0.49	11	NA	NA	14000	
		PO/5[d]	NA	NA	11	5780	1.13	36200	52

[a]All experiments involving animals were conducted in our AAALAC-accredited facilities and were reviewed and approved by Pfizer Institutional Animal Care and Use Committee. Pharmacokinetic parameters were calculated from plasma concentration–time data and are reported as average values for n = 2. Maximum plasma concentrations (C_{max}) after PO dosing were determined directly from the experimental data, with T_{max} defined as the time of first occurrence of C_{max}. The area under the plasma concentration-time curve from t=0 to 24 h (AUC_{0-24}) was estimated using the linear trapezoidal rule. Oral bioavailability (F) was calculated from dose-normalized AUC_{PO}/AUC_{IV}. Systemic plasma clearance was calculated as the IV dose divided by the AUC obtained after IV dosing. Apparent steady-state volume of distribution (V_{ss}) was determined as the IV dose divided by the product of AUC and the elimination rate constant. Male Wistar Hann rats and male cynomolgus monkeys were used for IV (n = 2) and PO (n = 2) pharmacokinetic analysis. Unless otherwise noted, compounds were orally administered in crystalline free form as a suspension in 0.5% MC containing 0.1% tween80 and PO pharmacokinetics were examined in the fasted state in both species.
[b]**8** and **11** were administered IV as a solution in 10% DMSO/90% of 20% sulfobutylether-betacyclodextrin in water.
[c]**12** was administered IV as a solution in 10% DMSO/30% PEG400/60% water.

[d]**12** was administered as a tris(hydroxymethyl)aminomethane (tris) salt
[e]**12** was administered IV as a solution in 2% *N*-methylpyrrolidone and 98% sulfobutylether-betacyclodextrin (12.5%) in 50 mM TRIS buffer, pH 8.0.
[f]below the lower limit of detection (1 ng/mL). NA = not applicable; ND = not determined.

In Vitro Characterization of the Pharmacology of 12. A 96–well radioenzymatic assay that measured incorporation of [^{14}C]-bicarbonate into [^{14}C]-malonyl–CoA was used to examine the effect of **12** on purified human and rat ACC isozymes (ACC1 and ACC2) as previously described.[13] In substrate concentration-dependence experiments, compound **12** was found to be uncompetitive with ATP and noncompetitive with carbonate,[41] consistent with previously reported inhibitors binding in this pocket of the protein.[2] Dose-response experiments for inhibition of human and rat ACC isozymes were performed at saturating concentrations of ATP where the inhibitory concentration (IC_{50}) approximates the equilibrium dissociation constant for an enzyme (K_i) for uncompetitive inhibitors. The IC_{50} values for inhibition of human ACC1 and human ACC2 by **12** were determined to be 12.4 ± 1.4 nM and 8.66 ± 2.45 nM respectively.[41] Similarly, **12** inhibited rat ACC1 and ACC2 in a concentration-dependent manner with IC_{50} values of 7.53 ± 0.71 nM and 8.24 ± 4.13 nM, respectively.[41] The human ACC1 and ACC2 potencies of **12** in the radiometric assays were ~3-fold more potent than the corresponding values determined in the Transcreener® assays. Overall, the ACC inhibitory potency and mode of action of **12** was comparable to the values observed with the non-carboxylic acid derivative **3**.

In Vitro Disposition and Off-Target Activity Characterization of 12. Whether the OATP substrate properties of **12** translated into active hepatic uptake in primary human cells was addressed in incubations of **12** (1 μM) in sandwich-cultured human hepatocytes in the absence or presence of the OATP inhibitor rifamycin SV.[42] Significant active uptake of **12** was observed with an active to passive uptake clearance ratio of 8.7 (Table 6). Thus, **12** was likely to have

asymmetric liver distribution and an active uptake mediated systemic clearance in humans, consistent with its extended clearance classification system (ECCS) class 1B classification.[27] The OATP isoform OATP2B1 and the sodium-taurocholate cotransporting polypeptide (NTCP) are also expressed in the sinusoidal membrane of hepatocytes, and are capable of transporting anionic substrates into the liver.[25, 26] Therefore, we also examined the substrate properties of **12** for human OATP2B1 and human NTCP in vitro, using identical experimental conditions as the ones used for OATP1B1 and OATP1B3. The uptake ratio of **12** (1 μM) by OATP2B1 and NTCP in their corresponding HEK293 transfected cells was determined from 0.5–4.0 min at 37 °C. The uptake ratios (mean of ratios from 0.5–4.0 min) of **12**, which were obtained by dividing the uptake in transporter transfected cells by the HEK293-wild type uptake, were 7.0 and 3.2, for OATP2B1 and NTCP, respectively.

Table 6. Active Uptake of **12** (1 μM) in Sandwich-Cultured Human Hepatocytes[a]

	CL_{active} (μL/min/mg)	$CL_{passive}$ (μL/min/mg)[a]	Active/Passive Ratio
12	24	2.7	8.7

[a] CL_{active} and $CL_{passive}$ represent active uptake intrinsic clearance and passive diffusion clearance, respectively. $CL_{passive}$ of **12** was assessed in human hepatocyte incubations of **12** in the presence of 0.1 mM rifamycin SV (a pan-inhibitor of hepatic uptake transporters including OATPs). CL_{active} and $CL_{passive}$ were calculated by linear regression fitting of initial rate analysis in the presence or absence of rifamycin SV in sandwich-cultured human hepatocytes as previously outlined.[42]

Because **12** was resistant towards metabolic turnover ($CL_{int,met}$ < 3.0 μL/min/10^6 cells) in a two-hour human hepatocyte incubation, the $CL_{int,met}$ was reassessed in the human hepatocyte assay under relay conditions (~ 20 h), which extends drug residence time and provides reliable estimates of in vitro $CL_{int,met}$ for slowly metabolized compounds.[43] Using relay conditions, a $t_{1/2}$ value of ~ 540 min for the metabolic decline of **12** in human hepatocytes was observed, which

translated into a very low human $CL_{int,met}$ of 2.6 μL/min/10^6 cells. Preliminary metabolic profiling of **12** in human hepatocytes revealed trace levels of several metabolites derived from cytochrome P450 (CYP) mediated oxidations at the isopropyl group and/or the spirocycle region as well as a secondary alcohol metabolite derived from reduction of the carbonyl moiety. There were no human unique metabolites of **12**; all metabolites of **12** observed in human hepatocytes were also detected in hepatocytes from rat and monkey, which were the preclinical species for toxicological evaluation of **12**. Compound **12** exhibited high plasma protein binding in rat ($f_{u,p}$ = 0.0392), monkey ($f_{u,p}$ = 0.00956), and human ($f_{u,p}$ = 0.00600).

Compound **12** demonstrated no reversible inhibition (IC_{50} > 50 μM) of the major human CYP enzymes including CYP1A2, CYP2B6, CYP2C8, CYP2C9, CYP2C19, CYP2D6 and CYP3A4 in human liver microsomes.[44] In addition, **12** did not cause metabolism-dependent (time-, concentration- and NADPH-dependency) inhibition of major human CYPs in human liver microsomes, since there was a < 1.5-fold shift in the IC_{50} values for reversible inhibition and < 20% increase in inhibition of CYP activity upon preincubation of **12** in human liver microsomes in the presence or absence of the CYP co-factor NADPH.[45] Moreover, treatment of **12** (0.5–200 μM) in individual human hepatocytes lots did not lead to induction of messenger RNA and enzyme activity of CYP1A2 and CYP3A4, respectively. Reversible inhibition of major human uridine 5'-diphospho-glucuronosyltransferase (UGT) enzymes by **12** was also investigated in human liver microsomes using established protocols.[46] No inhibition (IC_{50} > 20 μM) of UGT1A4, UGT1A6, UGT1A9, UGT2B7, and UGT2B15 catalytic activities was observed with **12**.

The inhibitory potency of **12** for major human drug transporters was assessed in stably transfected cell-based transporter systems using well-established protocols.[38] Weak inhibition of

human multi-drug resistance protein (p-glycoprotein, ABCB1) and human breast cancer resistance protein (ABCG2) catalyzed efflux of its respective substrates, pitavastatin and digoxin, in MDCK-LE cell monolayers was observed with **12** providing IC_{50} values of 39 μM and 68 μM, respectively. Likewise, **12** demonstrated weak inhibitory effects on OATP1B1 and OATP1B3 mediated transport of rosuvastatin in HEK293 cells with IC_{50} values of 11.7 μM and 137 μM, respectively. Compound **12** did not demonstrate any inhibition (IC_{50} > 30 μM) of the uptake of *para*-aminohippuric acid and metformin by human renal transporters organic anion transporter 1 (SLC22A6) and 3 (SLC22A8) and organic cation transporter 2 (SLC22A2) in HEK293 cells. Collectively, these data suggest that **12** is unlikely to cause drug-drug interactions with drugs that are subject to active transport via intestinal, liver, or kidney transporters.

Compound **12** demonstrated high selectivity for ACC inhibition, with no significant off-target activity detected upon evaluation of **12** (at 100 μM) against a broad panel of transporters, receptors, ion channels and enzymes, including the hERG channel. In addition, **12** did not cause mutagenicity in the *Salmonella* Ames (strains TA98, TA100, TA1535 and TA1537) and in vitro micronucleus assays (in Chinese hamster ovary or thymidine kinase heterozygote TK6 cells) in the absence or presence of metabolic activation (aroclor-induced rat liver S9 fraction/NADPH). Finally compound **12** demonstrated very weak inhibition (IC_{50} = 94 μM) of the human bile salt export pump mediated transport of taurocholic acid in a membrane vesicle assay,[47] suggesting that **12** does not pose a risk of cholestatic liver injury due to impaired transport of cytotoxic bile salts.[48]

In Vivo Pharmacodynamics of 12 in Rats. Sprague-Dawley rats were utilized to quantify the effect of **12** on DNL in a tissue-specific manner by comparing the local incorporation of ^{14}C-labelled acetate into lipids, relative to vehicle treated animals. Single dose, PO administration of

12 resulted in dose-dependent reductions in liver DNL with a maximal reduction of 82% (EC_{50} = 5.4 nM (1.6-16.9 nM for 95% confidence interval)) at 300 mg/kg (corresponding to an unbound plasma concentration of 119.4 nM ± 57.2 at 300 mg/kg). In contrast, the maximal DNL inhibition observed in lung and bone marrow at this dose was 29 and 33%, respectively (Figure 3A). Collectively, these data demonstrate that the hepatoselective distribution of **12** results in greater DNL inhibition in liver relative to other tissues.

A

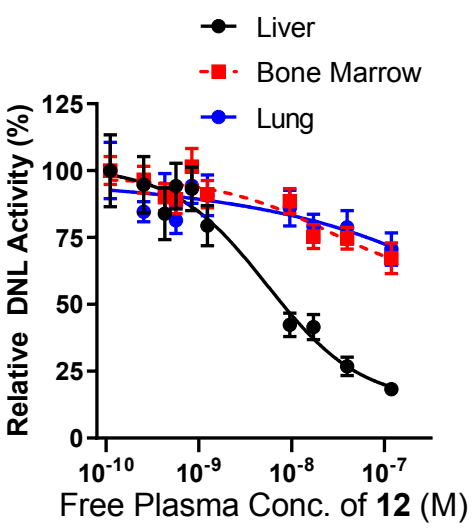

B

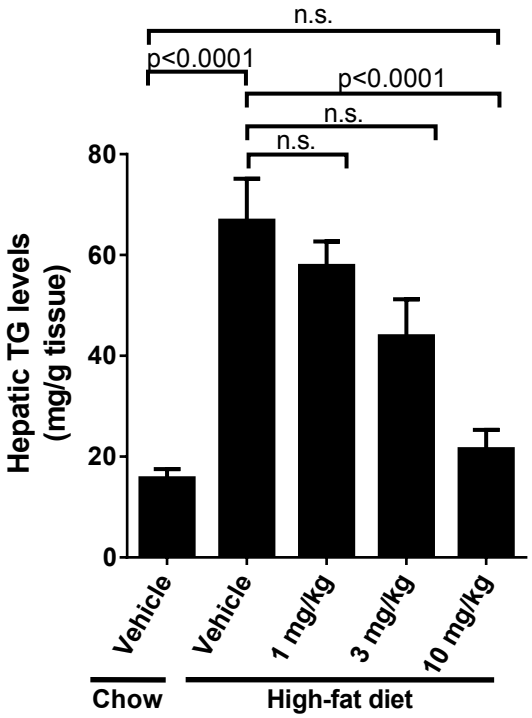

Figure 3. Pharmacodynamic evaluation of **12** in rats. (A) Dose dependent effect of orally administered **12** on DNL in liver, bone marrow, and lungs in rats relative to vehicle-treated animals (n = 16 animals per dose group, data reported as mean ± SEM) two hours post-dose. Administered PO doses of **12** were 0.03, 0.1, 0.3, 1, 3, 10, 30, 100 and 300 mg/kg, respectively. Vehicle was 0.5% methyl cellulose. (B) Dose dependent effect of chronic administration of **12**

on hepatic TG levels in rats fed a high-fat diet (n = 10 animals per dose group, data reported as mean ± SEM). n.s. = non-significant. SEM = standard error of the mean.

The effect of **12** on hepatic TG accumulation was also evaluated in Sprague-Dawley rats. Relative to chow fed rats, vehicle treated rats fed a high-fat diet showed an approximately six-fold increase in hepatic TG accumulation (Figure 3B). PO administration of **12** for 42 days to high-fat diet fed rats produced dose dependent reductions in hepatic TG levels, with the 10 mg/kg dose reducing hepatic TG to levels that are statistically similar to the hepatic TG levels observed in chow fed rats. Lower doses of **12** (1 and 3 mg/kg) demonstrated a trend towards lowering of hepatic TG levels by ~30% but this did not reach statistical significance ($p>0.05$).

In Vivo Pharmacodynamics and Safety Evaluation of 12 in NHPs. In order to measure the effect of **12** on hepatic DNL in NHPs, male cynomolgus macaques were administered D_2O and the correlation between plasma deuterium oxide and deuterium incorporation into plasma TG palmitate was measured. PO fructose administration has been found to increase both the rate of hepatic DNL and the reproducibility of DNL measures made between study periods.[49] For these reasons, the effect of **12** on hepatic DNL inhibition was assessed in NHPs concurrent to PO fructose administration. Following an overnight fast and enrichment of plasma deuterium oxide, fructose-loading resulted in significantly increased DNL in vehicle-treated animals (Figure 4). This increase in DNL was fully attenuated by PO administration of 10 mg/kg of **12** and complete inhibition of DNL persisted for the remainder of the nine-hour study.

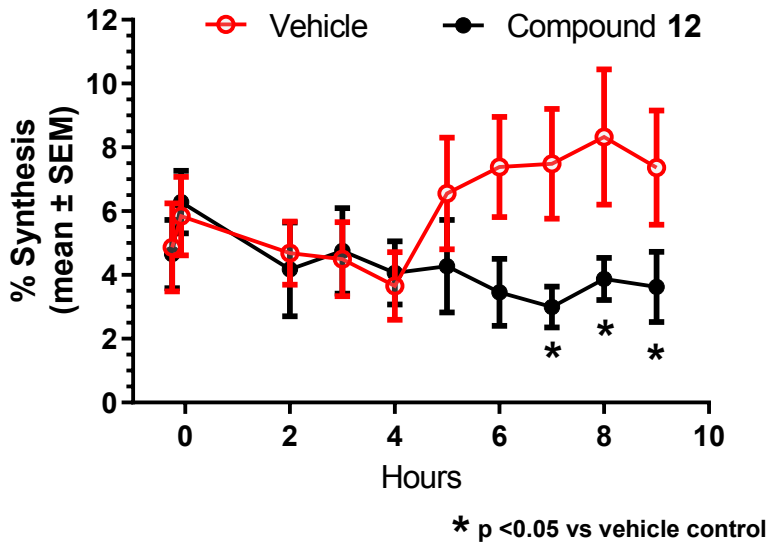

Figure 4. Effect of a single 10 mg/kg PO dose of **12** on fractional palmitate synthesis during fructose-simulated DNL in NHPs (n = 12 animals, data reported as MEAN ± SEM). *p <0.05 vs vehicle control. SEM = standard error of the mean. Fructose was given orally every 30 minutes beginning with dosing of **12** (t = 0). One banana was also given at hour 2 and 3.

Compound **12** was also orally administered to NHPs (n = 3/sex/dose) at doses of 3, 10, 30, and 90 mg/kg/day for 2 weeks and platelet counts were evaluated prior to the initiation of dosing and on dosing day 13. Administration of **12** at 3 or 10 mg/kg did not alter platelet count. However, at doses ≥30 mg/kg/day, mild decreases in platelet counts were observed in animals (Figure 5). The lowest absolute platelet count was 193,000/μL compared with concurrent control values ranging from 218,000 to 442,000/μL. Overall, these observations were consistent with the hepatoselectivity of **12**, where fructose-stimulated increase in hepatic DNL was blunted with administration of **12** at 10 mg/kg without any concomitant reduction in platelet count. The hypothesis that the hepatoselective attribute of **12** is expected to provide an improved therapeutic index in comparison to **3** for treating a liver disease such as NASH has been confirmed in a first-

in-human safety, tolerability, and pharmacokinetics study in healthy human subjects.[50, 51] In this study, compound **12** was well-tolerated in humans and doses that were associated with ~ 80% inhibition of liver DNL did not lead to statistically significant decreases in platelet counts following two weeks of daily dosing.[50, 51]

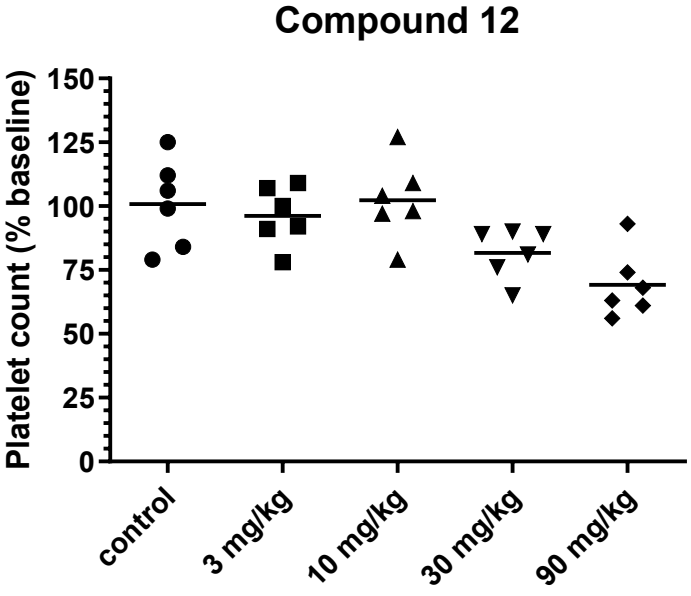

Figure 5. Change in platelets following 14 days of administration of compound **12** in NHPs.[14]

CHEMISTRY

Scheme 1. Synthesis of compound **4**[a]

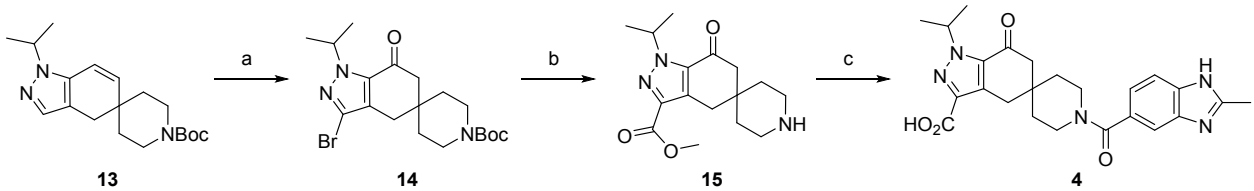

[a](a) i. NBS, MeOH, 44%; ii. KO*t*-Bu, THF, 80 °C; then 2 M HCl, quant.; (b) i. Pd(dppf)Cl_2, CO (1 mPa), MeOH, 100 °C, 78%; ii. TFA, CH_2Cl_2, 88%; (c) i. 2-methylbenzimidazole-5-carboxylic acid, HATU, NMM, THF, 37%; ii. Aq. LiOH, MeOH, 62%.

To synthesize pyrazole acid **4**, the previously-described olefin **13**[52] was treated with excess *N*-bromosuccinimide (NBS) in methanol which led to both bromination of the pyrazole and *O*-methyl bromohydrin formation (Scheme 1). Elimination to the enol ether with potassium *t*-butoxide followed by treatment with acid led to ketone **14**. The methyl ester was installed via Pd-catalyzed carbonylation and subsequent Boc removal led to amine **15**. Amide coupling followed by ester hydrolysis provided pyrazole acid **4**.

Scheme 2. Synthesis of compound **5**[a]

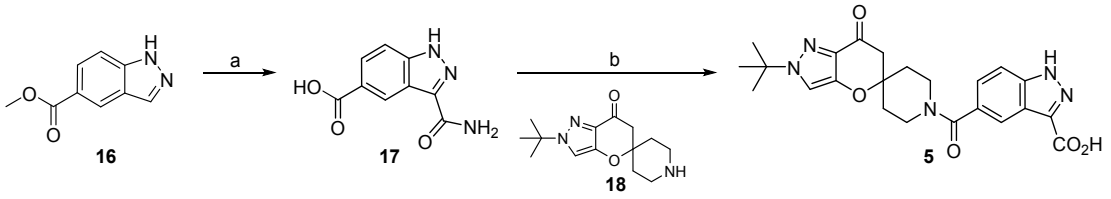

[a](a) i. K_2CO_3, I_2, DMF, 69%; ii. $Zn(CN)_2$, Zn, Pd(dppf)Cl_2, CuI, DMAc, 120 °C, quant.; iii. UHP, 2.5 M NaOH, MeOH, 77%. (b) i. **18**, EDC, HOBT, DMF, 70%; ii. $NOPF_6$, CH_3NO_2; then H_2O, 15%.

To access compound **5**, indazole acid **17** was first synthesized in a three-step sequence (Scheme 2). Indazole **16** was iodinated at the 3-position, copper-catalyzed cyanation was used to install the nitrile, and urea-hydrogen peroxide (UHP) and sodium hydroxide were used to hydrolyze the ester and nitrile to deliver indazole acid **17**. Standard amidation conditions were used to couple **17** to amine **18**.[11] Oxidative hydrolysis with nitrosonium hexafluorophosphate was used to

provide **5** (Scheme 2) as the indazole amide intermediate was resistant to base-mediated hydrolysis. Additionally, this method avoided a problematic opening of the spirochromanone that was observed upon exposure to aqueous strong base and competing hydrolysis of the central amide linkage.[52]

Scheme 3. Synthesis of compounds **6** and **7**[a]

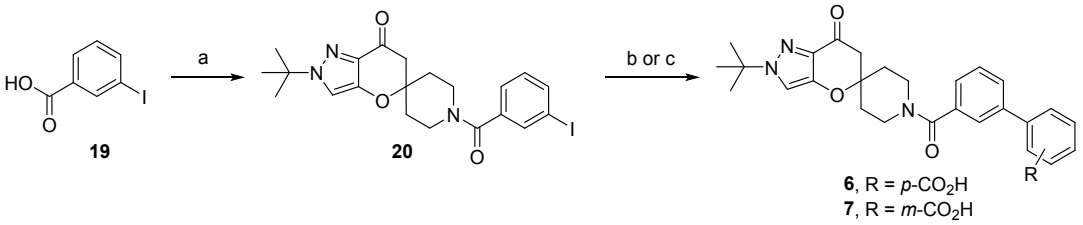

[a](a) i. $(COCl)_2$, DMF, CH_2Cl_2; ii. **18**, *i*-Pr_2NEt, CH_2Cl_2, 71% two steps; (b) 4-Carboxyphenylboronic acid, $Pd(PPh_3)_4$, aq. Na_2CO_3, DMF, Δ, 22%; (c) 3-Carboxyphenylboronic acid, $Pd(PPh_3)_4$, aq. Na_2CO_3, DMF, Δ, 33%.

In order to access the substituted biphenyl acids **6** and **7**, *m*-iodocarboxylic acid **19** was first coupled to spirocylic amine **18** via acid chloride formation to provide **20**. Suzuki coupling of iodide **20** with 4- and 3-carboxylphenylboronic acids directly led to **6** and **7**, respectively (Scheme 3).

Scheme 4. Synthesis of compounds **8**–**12**[a]

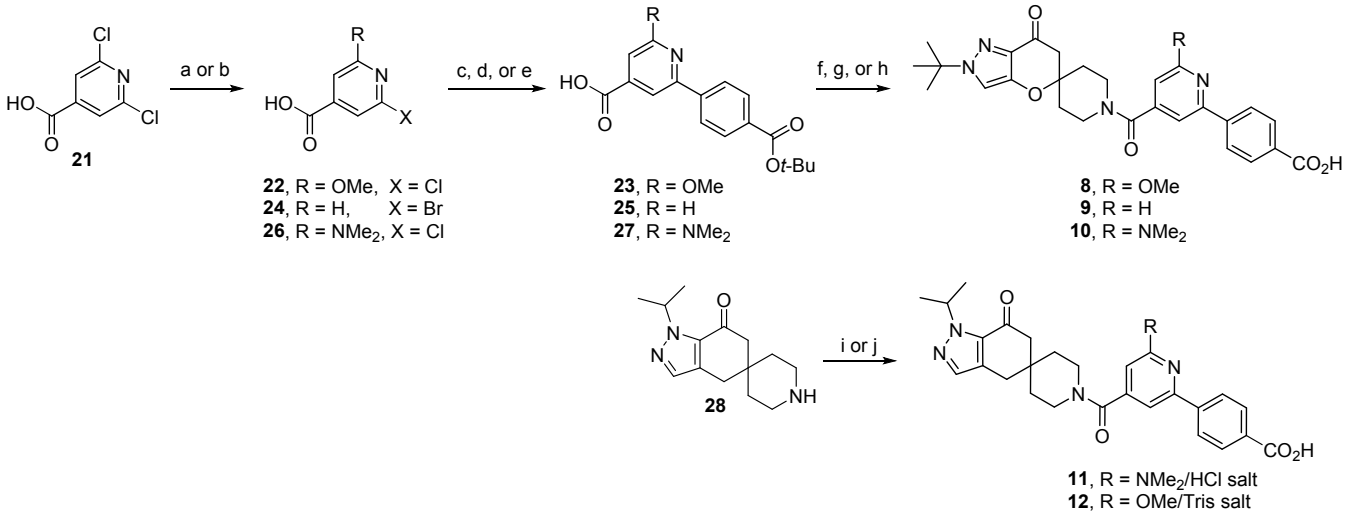

[a](a) 32% aq. NaOH, MeOH, 93%; (b) Me_2NH, THF, 80 °C, 90% (c) **22**, 4-(tert-butoxycarbonyl)phenylboronic acid, pinacol ester, $Pd(PPh_3)_4$, aq. Na_2CO_3, dioxane, 110 °C, 66%; (d) **24**, 4-(tert-butoxycarbonyl)phenylboronic acid, $Pd(dppf)Cl_2$, aq. K_3PO_4, dioxane, 70 °C, 20%; (e) **26**, 4-(tert-butoxycarbonyl)phenylboronic acid, $Pd(OAc)_2$, SPhos, aq. Na_2CO_3, dioxane, 95 °C, 65% or **26**, 4-(tert-butoxycarbonyl)phenylboronic acid, aq. Na_2CO_3, $Pd(dppf)Cl_2 \cdot CH_2Cl_2$, DME, 100–120 °C; (f) i. **18**, **23**, HATU, *i*-Pr_2NEt, CH_2Cl_2, quant.; ii. TFA, CH_2Cl_2, 92%; (g) **18**, **25**, EDC, HOBT, *i*-Pr_2NEt, DMF, 23–70 °C; ii. 4 M HCl in dioxane, 46% two steps, (h) i. **18**, **27**, EDC, HOBT, Et_3N, CH_2Cl_2; ii. TFA, CH_2Cl_2, 66% two steps; (i) i. **27**, EDC, HOBT, *i*Pr_2NEt, CH_2Cl_2, 48% over two steps; ii.4 M HCl in dioxane, CH_2Cl_2, MeOH, 55%; (j) i. CDI, THF; **23**, CH_2Cl_2, 50 °C, 82%; ii. H_3PO_4, $PhCH_3$, 50 °C, 52%; iii. $(HOCH_2)_3CNH_2$, EtOH, heptane, 92%.

The syntheses of pyridyl analogs **8–11** were completed through a three-step sequence (Scheme 4): (1) Suzuki coupling of halo-carboxylic acids **22**, **24**, or **26**, with the para-ester substituted phenylboronic acid or pinacol ester, (2) amidation with **18** or **28**,[52] and (3) acid-catalyzed hydrolysis of the *t*-butyl ester to reveal the carboxylic acid. To synthesize **12** on larger scale, acid

intermediate **22** was prepared from dichloropyridine **21** via S_NAr with sodium methoxide. To improve practicality, CDI was employed for the amide coupling between **23** and **28** and phosphoric acid was used for the ester hydrolysis to produce **12**. Tris(hydroxymethyl)aminomethane (Tris) was then used to produce the salt of **12**.

CONCLUSIONS

Reductions in platelet count were observed in previous clinical studies evaluating ACC inhibitor **3**. These reductions were demonstrated to result from ACC inhibition in bone marrow leading to impaired platelet production. The design of hepatoselective compounds was pursued as a strategy to improve the safety profile of ACC inhibitors. Starting with ACC inhibitors **2** and **3**, a series of analogs was prepared by incorporating a biaryl motif appended with a carboxylic acid to infer OATP recognition and active transport into hepatocytes. This effort led to the identification of ACC inhibitor PF-05221304 (**12**) which exhibited both a high level of hepatoselectivity and passive permeability, and good oral bioavailability in animals. The good oral absorption of **12** in animals when coupled with its very low metabolic clearance in human hepatocytes suggest that **12** may be suitable for administration to humans in a once daily dosing paradigm with little-to-no risks of drug-drug interactions with concomitantly administered medications. The liver exposure of **12** led to significant and selective DNL inhibition in the liver relative to other tissues, providing an efficacious and safe profile in preclinical species. Based on its overall disposition and safety profile, **12** was progressed to clinical trials and demonstrated an attractive safety, tolerability, pharmacokinetic, and pharmacodynamic profile in humans following administration of single- and multiple-ascending doses.[51]

EXPERIMENTAL SECTION

General. Unless otherwise noted, the reported experiments followed these considerations: All chemicals, reagents, and solvents were purchased from commercial sources when available and used without further purification. Reactions were magnetically stirred, and monitored by thin layer chromatography, liquid chromatography-mass spectrometry (LCMS), and/or high performance liquid chromatography (HPLC). Reactions were carried out at room temperature (~23 °C) unless otherwise noted. Air and moisture-sensitive were carried out under an atmosphere of nitrogen. Silica gel chromatography was performed using an Isco or Biotage automated purification system with pre-packaged columns. Concentration under reduced pressure (in vacuo) was performed by rotary evaporation at 25–45 °C. Purified compounds were further dried under high vacuum with or without heat to remove residual solvent. ^{1}H NMR spectra were obtained with a spectrometer at 600 MHz or 400 MHz. Chemical shifts were referenced to the residual ^{1}H solvent signals ($CDCl_3$, δ 7.27; DMSO-d_6, δ 2.50; CD_3OD, δ 3.31). Signals are listed as follows: chemical shift in ppm; multiplicity identified as br, broad; s, singlet; d, doublet; t, triplet; q, quartet; spt, septet. m, multiplet; coupling constants (*J*) in Hz.

All compounds evaluated were > 95% pure. Specific interaction between this chemical series and ACC is supported by co-crystal structures such as the one reported with compound **2**.[13]

Synthesis of analogs and intermediates

*tert-Butyl 3-bromo-1-isopropyl-7-oxo-1,4,6,7-tetrahydrospiro[indazole-5,4'-piperidine]-1'-carboxylate (**14**)*. Step 1: **13**[52] (1 g, 3 mmol) in MeOH (20 mL) was added NBS (1.6 g, 9.0 mmol). The mixture was stirred at rt for 1 h then concentrated in vacuo. The residue was dissolved in ethyl acetate, then washed with saturated sodium thiosulfate, 0.5 M NaOH (20 mL), brine, and concentrated in vacuo. The resulting oil was purified by flash column chromatography

(petroleum ether:ethyl acetate, 10:1) to provide tert-butyl 3,6-dibromo-1-isopropyl-7-methoxy-1,4,6,7-tetrahydrospiro[indazole-5,4'-piperidine]-1'-carboxylate (730 mg, 44%) as a colorless oil. ^{1}H NMR (400 MHz, $CDCl_3$) δ 4.70 (d, *J*=1.5 Hz, 1H), 4.40 (s, 1H), 4.29 (spt, *J*=6.7 Hz, 1H), 3.77–3.66 (m, 1H), 3.63-3.53 (m, 4H), 3.25 (ddd, *J*=3.5, 10.3, 13.3 Hz, 1H), 3.14 (ddd, *J*=3.5, 9.8, 13.8 Hz, 1H), 2.57 (d, *J*=16.1 Hz, 1H), 2.35 (d, *J*=16.1 Hz, 1H), 1.80-1.63 (m, 4H), 1.51 (d, *J*=6.5, 3H), 1.48 (d, *J*=6.5, 3H), 1.46 (s, 9H).

Step 2: To a solution of tert-butyl 3,6-dibromo-1-isopropyl-7-methoxy-1,4,6,7-tetrahydrospiro[indazole-5,4'-piperidine]-1'-carboxylate (760 mg, 1.46 mmol) in THF (20 mL) was added KOtBu (340 mg, 3.03 mmol). The mixture was stirred at 80 °C for 15 h. HCl (2 M, 20 mL) was added to the solution and the mixture was stirred at rt for 3 h. The reaction was concentrated in vacuo. The resulting residue was dissolved in ethyl acetate and washed with water (20 mL) and brine then concentrated in vacuo. Flash column chromatography (petroleum ether:ethyl acetate, 10:1) was used to provide **14** (620 mg, quant.) as a colorless oil. ^{1}H NMR (400 MHz, $CDCl_3$) δ 5.36 (spt, *J*=6.6 Hz, 1H), 3.55–3.44 (m, 2H), 3.44–3.30 (m, 2H), 2.65 (s, 2H), 2.54 (s, 2H), 1.71–1.38 (m, 19H).

*Methyl 1-isopropyl-7-oxo-1,4,6,7-tetrahydrospiro[indazole-5,4'-piperidine]-3-carboxylate-TFA (**15**).* Step 1: To a solution of **14** (300 mg, 0.70 mmol) in MeOH (10 mL) was added $Pd(dppf)Cl_2$ (20 mg, 0.027 mmol). The mixture was degassed for 10 min, filled with carbon monoxide (1 mPa), and heated to 100 °C for 15 h. The reaction was concentrated in vacuo and purified via flash column chromatography (petroleum ether:ethyl acetate, 15:1) to provide 1'-(tert-butyl) 3-methyl 1-isopropyl-7-oxo-1,4,6,7-tetrahydrospiro[indazole-5,4'-piperidine]-1',3-dicarboxylate

(220 mg, 78%) as a colorless oil. ^{1}H NMR (400 MHz, $CDCl_3$) δ 5.45 (spt, *J*=6.6 Hz, 1H), 3.94 (s, 3H), 3.51–3.35 (m, 4H), 3.05 (s, 2H), 2.55 (s, 2H), 1.53–1.48 (m, 10H), 1.44 (s, 9H).

Step 2: 1'-(tert-butyl) 3-methyl 1-isopropyl-7-oxo-1,4,6,7-tetrahydrospiro[indazole-5,4'-piperidine]-1',3-dicarboxylate (220 mg, 0.540 mmol) was added to 1:1 TFA:CH_2Cl_2 (10 mL) and the mixture was stirred at rt for 3 h. The reaction was concentrated in vacuo to provide **15** (200 mg, 88%) which was used into next step without further purification.

*1-Isopropyl-1'-(2-methyl-1H-benzo[d]imidazole-5-carbonyl)-7-oxo-1,4,6,7-tetrahydrospiro[indazole-5,4'-piperidine]-3-carboxylic acid (**4**).* Step 1: To a solution of 2-methylbenzimidazole-5-carboxylic acid (200 mg, 1.13 mmol) in THF (10 mL) was added HATU (570 mg, 1.50 mmol) and the mixture was stirred at rt for 30 min. Compound **15** (300 mg, 1 mmol) and NMM (300 mg, 1 mmol) were then added and the reaction stirred for 3 h. The reaction was concentrated in vacuo and reverse-phase preparative HPLC was used to provide methyl 1-isopropyl-1'-(2-methyl-1H-benzo[d]imidazole-5-carbonyl)-7-oxo-1,4,6,7-tetrahydrospiro[indazole-5,4'-piperidine]-3-carboxylate (170 mg, 37%) as a white solid. ^{1}H NMR (400 MHz, CD_3OD) δ 7.68–7.42 (m, 2H), 7.27 (dd, *J*=1.5, 8.5 Hz, 1H), 5.46 (spt, *J*=6.7 Hz, 1H), 3.93 (s, 3H), 3.91–3.65 (m, 2H), 3.64–3.44 (m, 2H), 3.13 (s, 2H), 2.70 (s, 2H), 2.58 (s, 3H), 1.78–1.50 (m, 4H), 1.46 (d, *J*=7.0 Hz, 6H).

Step 2: A round bottom flask was charged with methyl 1-isopropyl-1'-(2-methyl-1H-benzo[d]imidazole-5-carbonyl)-7-oxo-1,4,6,7-tetrahydrospiro[indazole-5,4'-piperidine]-3-carboxylate (120 mg, 0.26 mmol) and 1:1 MeOH:water (6 mL). Lithium hydroxide (100 mg, 2.6 mmol) was then added and the reaction was stirred at rt for 15 h. The reaction was concentrated in vacuo. The residue was acidified to pH 5 and dried in vacuo to give a residue, which was

purified by preparative reverse-phase HPLC to provide **4** (85 mg, 62%) as a white solid. ^{1}H NMR (400 MHz, CD_3OD) δ 7.69 (s, 1H), 7.67 (d, *J*=8.5 Hz, 1H), 7.45 (dd, *J*=1.5, 8.5 Hz, 1H), 5.51–5.41 (m, 1H), 3.96–3.68 (m, 2H), 3.62–3.39 (m, 2H), 3.15 (s, 2H), 2.73 (s, 3H), 2.69 (br s, 2H), 1.81–1.53 (m, 4H), 1.47 (d, *J*=6.5 Hz, 6H). LCMS calc. for $C_{24}H_{27}N_5O_4(M+H)^+$: 450.2; found: 450.3. HPLC: 99.5%

*3-Carbamoyl-1H-indazole-5-carboxylic acid (**17**).* Step 1: A round bottom flask was charged with methyl 1H-indazole-5-carboxylate (25.9 g, 147 mmol) and DMF (200 mL) and stirred to dissolve. Potassium carbonate (57.3 g, 414 mmol) was added. Iodine (41.0 g, 162 mmol) in DMF (150 mL) was added dropwise to the stirring solution and the reaction was stirred at rt for 15 h. Water (800 mL) was added to the reaction mixture which resulted in a precipitate. A solution of sodium bisulfite (47.4 g, 456 mmol) in 150 mL of water and was added slowly to the stirring reaction mixture. The reaction mixture was stirred for 1 h. The precipitate was filtered and combined with solid from a similar scale batch. The solids were washed with 400 mL of water and 200 mL of heptane and dried for 1 h under vacuum to provide methyl 3-iodo-1H-indazole-5-carboxylate (67.5g, 69%). ^{1}H NMR (400 MHz, DMSO-d_6) δ 13.85 (s, 1H), 8.07 (s, 1H), 7.99 (dd, *J*=1.6, 8.8 Hz, 1H), 7.66 (dd, *J*=0.6, 8.8 Hz, 1H), 3.89 (s, 3H).

Step 2: A 1 L round bottom flask was charged with methyl 3-iodo-1H-indazole-5-carboxylate (31.75 g, 105.1 mmol), zinc cyanide (21.0 g, 179 mmol), zinc dust (4.2 g, 64 mmol), $Pd(dppf)Cl_2$ (13 g, 15 mmol), and copper iodide (20.4 g, 107 mmol). DMAc (500 mL) was added and the reaction mixture was purged with nitrogen for 10 min then heated to 120 °C for 1 h. The reaction was cooled to rt and diluted with ethyl acetate (1000 mL) and stirred for 20 min. The reaction mixture was filtered through a celite plug and washed with 500 mL of ethyl acetate. The filtrate

was added to a solution of saturated ammonium chloride/conc. ammonium hydroxide buffered solution (pH = 8, 2.0 L) and the biphasic solution was stirred vigorously for 1 h and filtered through a celite plug. The layers were separated, and the aqueous layer was washed with ethyl acetate (2 x 1.5 L). The combined organic layers were washed with water (900 mL x 2), brine (900 mL), dried over sodium sulfate, filtered and concentrated in vacuo. MeOH (100 mL) was added and the mixture was stirred for 20 min then filtered and washed with MeOH (10 mL). The filtrate was combined with another similar sized batch and concentrated under reduced pressure to provide methyl 3-cyano-1H-indazole-5-carboxylate (57.87 g, quant.) as a solid (contaminated with 1 equiv. DMAc). ^{1}H NMR (400 MHz, DMSO-d_6) δ 8.47 (s, 1H), 8.07 (dd, J=1.5, 8.9 Hz, 1H), 7.87 (d, J=9.0 Hz, 1H), 3.91 (s, 3H).

Step 3: A round bottom flask was charged with methyl 3-cyano-1H-indazole-5-carboxylate (50.0 g, 249 mmol) and MeOH (950 mL). The reaction was cooled to 10 °C and a solution of urea-hydrogen peroxide (241 g, 2.49 mol) in NaOH (2.5 M, 1.0 L) and water (100 mL) was added dropwise via an addition funnel at a rate to keep the internal temperature < 25 °C. The cooling bath was removed, and reaction was stirred at rt for 16 h. The reaction was cooled to 15 °C and solid urea-hydrogen peroxide (50.0 g, 532 mmol) was added in portions. Vigorous bubbling occurred during the addition and the reaction was stirred at rt for 2 h. Solids were removed via filtration and the filtrate was concentrated in vacuo to remove MeOH. The resultant solution was transferred to a 5 L flask and cooled in an ice bath. HCl (6 M, 420 mL) was added dropwise to adjust pH to 4. The mixture was stirred for 20 min and the solids were collected via filtration and dried in vacuo. The solids were triturated with 1:1 acetonitrile:dichloromethane (1.4 L) for 1 h, collected via filtration, and washed with 1:1 acetonitrile:dichloromethane to provide **17** (39.35 g, 77%) as a tan solid contaminated with urea (25 mol%). ^{1}H NMR (400 MHz, DMSO-d_6) δ 13.84

(s, 1H), 12.86 (br. s, 1H), 8.85 (br. s, 1H), 7.96 (dd, *J*=1.6, 8.8 Hz, 1H), 7.85 (br. s, 1H), 7.67 (d, *J*=8.8 Hz, 1H), 7.47 (br. s, 1H). LCMS calc. for $C_9H_7N_3O_3(M-H)^-$: 204.0; found: 204.0.

*5-(2'-(tert-Butyl)-7'-oxo-6',7'-dihydro-2'H-spiro[piperidine-4,5'-pyrano[3,2-c]pyrazole]-1-carbonyl)-1H-indazole-3-carboxylic acid (**5**).* Step 1: A round bottom flask was charged with **17** (195 mg, 0.949 mmol), **18** dihydrochloride (250 mg, 0.949 mmol), EDC (273 mg, 1.42 mmol), HOBT (192 mg, 1.42 mmol), and DMF (8 mL). The reaction was stirred at rt for 15 min. Triethylamine (384 mg, 3.80 mmol) was added in portions and the reaction was stirred at rt for 16 h. The mixture was diluted with water (30 mL) and saturated aqueous ammonium chloride (15 mL) then extracted with ethyl acetate (30 mL x 3). The combined organic layers were washed with brine, dried over sodium sulfate, filtered, and concentrated in vacuo. Flash column chromatography (1-5% MeOH in dichloromethane) was used to provide 5-(2'-(tert-Butyl)-7'-oxo-6',7'-dihydro-2'H-spiro[piperidine-4,5'-pyrano[3,2-c]pyrazole]-1-carbonyl)-1H-indazole-3-carboxamide (300 mg, 70%) as a yellow solid. ^{1}H NMR (400 MHz, CD_3OD) δ 8.33 (s, 1H), 7.67 (d, *J*=8.8 Hz, 1H), 7.61 (s, 1H), 7.50 (dd, *J*=1.5, 8.5 Hz, 1H), 4.57–4.38 (m, 1H), 3.76–3.37 (m, 3H), 2.77 (s, 2H), 2.31–1.93 (m, 2H), 1.92–1.67 (m, 2H), 1.58 (s, 9H).

Step 2: A round bottom flask was charged with 5-(2'-(tert-butyl)-7'-oxo-6',7'-dihydro-2'H-spiro[piperidine-4,5'-pyrano[3,2-c]pyrazole]-1-carbonyl)-1H-indazole-3-carboxamide (300 mg, 0.67 mmol) and nitromethane (10 mL) then cooled to 0 °C. Nitrosonium hexafluorophosphate (186 mg, 1.07 mmol) was then added and the reaction was stirred at rt for 15 h. The reaction was quenched with the addition of water and the pH was adjusted to 4 with aqueous sodium bicarbonate solution. Ethyl acetate was added and the mixture was separated. The aqueous layer was extracted with ethyl acetate (x 3) and the combined organic layers were washed with brine,

dried over sodium sulfate, filtered, and concentrated in vacuo. The material was purified twice with preparative reverse phase HPLC to provide **5** (45 mg, 15%). ^{1}H NMR (400 MHz, CD_3OD) δ 8.37 (s, *J*=6.1 Hz, 1H), 7.64–7.59 (m, 2H), 7.44 (d, *J*=8.5 Hz, 1H), 4.55–4.39 (m, 1H), 3.85–3.64 (m, 1H), 3.62–3.31 (m, 2H), 2.77 (br. s, 2H), 2.30–1.94 (m, 2H), 1.92–1.71 (m, 2H), 1.58 (s, 9H). LCMS calc. for $C_{23}H_{25}N_5O_5(M-H)^-$: 450.2; found: 450.3. HPLC: 99.51%

*2'-(tert-Butyl)-1-(3-iodobenzoyl)-2'H-spiro[piperidine-4,5'-pyrano[3,2-c]pyrazol]-7'(6'H)-one (**20**).* To a solution of 3-iodobenzoic acid (1.5 g, 6.0 mmol) in anhydrous dichloromethane (5 mL) was added oxalyl chloride (0.75 g, 5.9 mmol) dropwise at 0 °C, followed by one drop of dimethylformamide. The solution was stirred at room temperature for 6 h and then concentrated in vacuo to a residue which was diluted in anhydrous dichloromethane (8 mL). **18** dihydrochloride (1.5 g, 5.7 mmol) was then added followed by Hünig's base (7.7 g, 60 mmol). The solution was then stirred at room temperature for 12 h. The mixture was poured onto water and extracted with dichloromethane (10 mL x 3). The combined organic layers were dried over sodium sulfate, filtered, concentrated in vacuo, and purified by column chromatography to provide **20** (2.0 g, 71%) as a white solid. ^{1}H NMR (400 MHz, $CDCl_3$) δ 7.80–7.71 (m, 2H), 7.36 (td, *J*=1.0, 7.8 Hz, 1H), 7.25 (s, 1H), 7.15 (t, *J*=7.5 Hz, 1H), 4.57–4.39 (m, 1H), 3.63–3.36 (m, 2H), 3.34–3.13 (m, 1H), 2.70 (d, *J*=3 Hz, 2H), 2.30–1.99 (m, 2H), 1.81–1.54 (m, 2H), 1.61 (s, 9H). LCMS calc. for $C_{21}H_{24}IN_3O_3$ $(M+H)^+$: 493.1; found: 494.3.

*3'-(2'-(tert-Butyl)-7'-oxo-6',7'-dihydro-2'H-spiro[piperidine-4,5'-pyrano[3,2-c]pyrazole]-1-carbonyl)-[1,1'-biphenyl]-4-carboxylic acid (**6**).* A mixture of **20** (0.2 g, 0.4 mmol), 4-carboxyphenylboronic acid (67 mg, 0.38 mmol), $Pd(PPh_3)_4$ (25 mg, 0.019 mmol), and sodium carbonate (108 mg, 0.72 mmol) in DMF/water (2 mL/2 mL) was heated to reflux for 12 h. The

mixture was poured onto water and extracted with dichloromethane (10 mL x 3). The combined organic layers were dried over sodium sulfate, concentrated in vacuo, and purified by preparative reverse phase HPLC to provide **6** (40 mg, 22%) as a white solid. ^{1}H NMR (400 MHz, $CDCl_3$) δ 8.17 (d, *J*=7.0 Hz, 2H), 7.75–7.63 (m, 4H), 7.52 (t, *J*=7.5 Hz, 1H), 7.43 (d, *J*=7.5 Hz, 1H), 7.25 (s, 1H), 4.64–4.47 (m, 1H), 4.20–3.20 (m, 4H), 2.72 (br. s, 2H), 2.35–1.98 (m, 2H), 1.85–1.70 (m, 1H), 1.60 (s, 9H), 1.67–1.52 (m, 1H). LCMS calc. for $C_{28}H_{29}N_3O_5$ $(M+H)^+$: 488.2; found: 488.6. HPLC: 95.58%.

3'-(2'-(tert-Butyl)-7'-oxo-6',7'-dihydro-2'H-spiro[piperidine-4,5'-pyrano[3,2-c]pyrazole]-1-carbonyl)-[1,1'-biphenyl]-3-carboxylic acid (7). A mixture of **20** (0.2 g, 0.4 mmol), 3-carboxyphenylboronic acid (67 mg, 0.38 mmol), $Pd(PPh_3)_4$ (25 mg, 0.019 mmol), and sodium carbonate (108 mg, 0.72 mmol) in DMF/water (2 mL/2 mL) was heated to reflux for 12 h. The mixture was poured onto water and extracted with dichloromethane (10 mL x 3). The combined organic layers were dried over sodium sulfate, concentrated in vacuo, and purified by preparative reverse phase HPLC to provide **7** (60 mg, 33%) as a white solid. ^{1}H NMR (400 MHz, $CDCl_3$) δ 8.35 (s, 1H), 8.10 (d, *J*=7.5 Hz, 1H), 7.81 (d, *J*=8.0 Hz, 1H), 7.71 (s, 1H), 7.68 (d, *J*=8.0 Hz, 1H), 7.59–7.47 (m, 2H), 7.41 (d, *J*=7.4 Hz, 1H), 7.25 (s, 1H), 5.07 (br. s, 1H), 4.64–4.51 (m, 1H), 3.76–3.20 (m, 3H), 2.72 (d, *J*=2.5 Hz, 2H), 2.36–1.98 (m, 2H), 1.87–1.69 (m, 1H), 1.69–1.54 (m, 1H), 1.60 (s, 9H). LCMS calc. for $C_{28}H_{29}N_3O_5$ $(M+H)^+$: 488.2; found: 488.5. HPLC: 98.03%.

*2-chloro-6-methoxyisonicotinic acid (**22**)* A round bottomed flask was charged with 2,6-dichloroisonicotinic acid (230 g, 1.20 mol) and MeOH (2.5 L). 32% aqueous NaOH (500 mL) was added and the reaction was stirred at 80 °C for 12 h. The reaction was cooled to rt and concentrated in vacuo to remove MeOH. The residue was diluted with water (500 mL), acidified

to pH 3 with 1 M HCl and stirred for 10 min. Ethyl acetate (500 mL) was added and the layers were separated. The aqueous layer was extracted with ethyl acetate (500 mL x 2) and the combined organic layers were washed with brine, dried over magnesium sulfate, filtered, and concentrated in vacuo to provide **22** (210 g, 93%) as a white solid. ^{1}H NMR (400 MHz, DMSO-d_6) δ 7.39 (s, 1H), 7.18 (s, 1H), 3.90 (s, 3H).

*2-(4-(tert-Butoxycarbonyl)phenyl)-6-methoxyisonicotinic acid (**23**).* A round bottom flask was charged with **23** (175 g, 0.933 mol), 4-(tert-butoxycarbonyl)phenylboronic acid, pinacol ester (340.7 g, 1.12 mol), and dioxane (6.0 L). Sodium carbonate (297 g, 2.80 mol) in water (2.0 L) was added and the reaction stirred for 5 min. $Pd(PPh_3)_4$ (37.7 g, 32.6 mmol) was added and the reaction was heated to 110 °C for 16 h. The reaction was cooled to rt and concentrated in vacuo to a minimal volume to give a very thick dark brown suspension. The suspension was combined with ethyl acetate (4.0 L) and water (2.0 L) and stirred for 5 min. The layers were separated and aqueous layer was extracted with ethyl acetate (1 L x 3). The combined organic layers were washed with 1 M HCl, brine, dried over magnesium sulfate, filtered, and concentrated in vacuo to a reduced volume. When solid had formed, the mixture was filtered and washed with 1:1 ethyl acetate:petroleum ether (200 mL). The collected solids were dried in vacuo to provide **23** (202 g, 66%) as a yellow solid. ^{1}H NMR (600 MHz, DMSO-d_6) δ 13.77 (br. s, 1H), 8.25 (d, *J*=8.2 Hz, 2H), 8.01 (d, *J*=8.2 Hz, 2H), 7.97 (s, 1H), 7.22 (s, 1H), 4.02 (s, 3H), 1.57 (s, 9H). LCMS calc. for $C_{18}H_{19}NO_5$ $(M+H)^+$: 330.1; found: 330.2.

*4-(4-(2'-(tert-Butyl)-7'-oxo-6',7'-dihydro-2'H-spiro[piperidine-4,5'-pyrano[3,2-c]pyrazole]-1-carbonyl)-6-methoxypyridin-2-yl)benzoic acid (**8**).* Step 1: A round bottom flask was charged with **18** dihydrochloride (350 mg, 1.17 mmol), **23** (384 mg, 1.17 mmol) and dichloromethane (25

mL). HATU (488 mg, 1.28 mmol) was added followed by Hünig's base (0.61 mL, 3.5 mmol) and the reaction was stirred for 2 days. The reaction was concentrated in vacuo and purified via flash column chromatography to tert-butyl 4-(4-(2'-(tert-butyl)-7'-oxo-6',7'-dihydro-2'H-spiro[piperidine-4,5'-pyrano[3,2-c]pyrazole]-1-carbonyl)-6-methoxypyridin-2-yl)benzoate (705 mg, quant) as a white foam. ^{1}H NMR (400 MHz, $CDCl_3$) δ 8.08 (s, 4H), 7.37 (d, *J*=0.8 Hz, 1H), 7.25 (s, 1H), 6.69 (d, *J*=1.0 Hz, 1H), 4.59–4.44 (m, 1H), 4.07 (s, 3H), 3.61–3.40 (m, 2H), 3.31–3.21 (m, 1H), 2.76–2.65 (m, 2H), 2.30–2.21 (m, 1H), 2.13–2.05 (m, 1H), 1.81–1.68 (m, 1H), 1.66–1.54 (m, 1H), 1.63 (s, 9H), 1.61 (s, 9H). LCMS calc. for $C_{32}H_{38}N_4O_6$ $(M+H)^+$: 575.3; found: 575.6.

Step 2: A round bottom flask was charged with tert-butyl 4-(4-(2'-(tert-butyl)-7'-oxo-6',7'-dihydro-2'H-spiro[piperidine-4,5'-pyrano[3,2-c]pyrazole]-1-carbonyl)-6-methoxypyridin-2-yl)benzoate **(**700 mg, 1.22 mmol), dichloromethane (15 mL), and TFA (5 mL) and the reaction was stirred at rt for 15 h. The reaction was concentrated in vacuo and purified via flash column chromatography (ethyl acetate/heptane with 0.5% acetic acid). The pure material was triturated with MTBE (30 mL) and heptane (50 mL) and filtered to provide **8** (583 mg, 92%) as a white solid. ^{1}H NMR (400 MHz, $CDCl_3$) δ 8.23–8.12 (m, 4H), 7.41 (d, *J*=0.8 Hz, 1H), 7.25 (s, 1H), 6.72 (d, *J*=0.8 Hz, 1H), 4.59–4.51 (m, 1H), 4.08 (s, 3H), 3.63–3.41 (m, 2H), 3.35–3.25 (m, 1H), 2.77–2.66 (m, 2H), 2.32–2.19 (m, 1H), 2.16–2.04 (m, 1H), 1.83–1.70 (m, 1H), 1.66–1.55 (m, 1H), 1.61 (s, 9H). LCMS calc. for $C_{28}H_{30}N_4O_6$ $(M+H)^+$: 519.2; found: 519.6.

*2-(4-(tert-Butoxycarbonyl)phenyl)isonicotinic acid (**25**).* To a vial was added **24** (203 mg, 1.00 mmol), 4-(tert-butoxycarbonyl)phenylboronic acid (312 mg, 1.41 mmol), potassium phosphate (639 mg, 3.01 mmol), dioxane (3 mL) and water (1 mL) at rt. The solution was purged with

nitrogen for 5 min followed by addition of $Pd(dppf)Cl_2$ (73 mg, 0.10 mmol) and additional purging for 1 minute. The reaction was heated at 70 °C for 64 h. The reaction was concentrated in vacuo to remove dioxane and ethyl acetate and 1M HCl were added. The layers were separated and the aqueous was extracted ethyl acetate x 2. The combined organic layers were dried, filtered, concentrated in vacuo, and purified by column chromatograph (0 to 6% MeOH in dichloromethane) to provide **25** (60 mg, 20%) as a yellow solid. LCMS calc. for $C_{17}H_{17}NO_4$ $(M+H)^+$:300.1; found: 300.1.

*4-(4-(2'-(tert-Butyl)-7'-oxo-6',7'-dihydro-2'H-spiro[piperidine-4,5'-pyrano[3,2-c]pyrazole]-1-carbonyl)pyridin-2-yl)benzoic acid (**9**).* Step 1: A vial was charged with **25** (30 mg, 0.10 mmol), **18** dihydrochloride (30 mg, 0.10 mmol), EDC (23 mg, 0.12 mmol), HOBT (16 mg, 0.12 mmol), and DMF (0.5 mL). Hünig's base (70 µL, 0.40 mmol) was then added and the reaction was stirred at rt for 18 h and 70 °C for 2 h. The reaction was cooled to rt and concentrated in vacuo. Ethyl acetate and water were added, the layers separated. The organic layer was washed with water, dried over sodium sulfate, filtered, and concentrated in vacuo. Flash column chromatography (15% ethyl acetate/heptane) was used to provide tert-butyl 4-(4-(2'-(tert-butyl)-7'-oxo-6',7'-dihydro-2'H-spiro[piperidine-4,5'-pyrano[3,2-c]pyrazole]-1-carbonyl)pyridin-2-yl)benzoate (33 mg, 60%) as a light brown oil. ^{1}H NMR (400 MHz, $CDCl_3$) □ 8.79 (d, *J*=4.9 Hz, 1H) 8.12–8.03 (m, 4H) 7.77 (s, 1H) 7.27–7.23 (m, 2H) 4.60–4.50 (m, 1H) 3.57–3.45 (m, 2H) 3.34–3.23 (m, 1H) 2.78–2.65 (m, 2H), 2.31–2.23 (m, 1H) 2.14–2.06 (m, 1H) 1.82–1.70 (m, 1H) 1.69–1.55 (m, 1H), 1.63 (s, 9H), 1.60 (s, 9H). LCMS calc. for $C_{31}H_{36}N_4O_5$ $(M+H)^+$: 545.3; found: 545.3

Step 2: A flask was charged with tert-butyl 4-(4-(2'-(tert-butyl)-7'-oxo-6',7'-dihydro-2'H-spiro[piperidine-4,5'-pyrano[3,2-c]pyrazole]-1-carbonyl)pyridin-2-yl)benzoate (32 mg, 0.060 mmol) and 4 mL of 4 N HCl in dioxane and stirred at rt for 18 h. The reaction was concentrated in vacuo and purified by preparative reverse phase HPLC to provide compound **9** (22 mg, 76%). LCMS calc. for $C_{27}H_{28}N_4O_5$ $(M+H)^+$: 489.2; found: 489.1. HPLC: 100%

*2-(4-(tert-Butoxycarbonyl)phenyl)-6-(dimethylamino)isonicotinic acid (**27**).* A flask was charged with 4-(tert-butoxycarbonyl)phenylboronic acid (648 mg, 2.92 mmol), **26** (450 mg, 2.24 mmol), dioxane (7.5 mL), and 2 N sodium carbonate (3.36 mL, 6.73 mmol). The mixture was bubbled with nitrogen for 10 min and palladium (II) acetate (20 mg, 0.090 mmol) and S-Phos (76 mg, 0.18 mmol) were added quickly. The reaction was heated to 95 °C for 5 h and cooled to room temp. The mixture was diluted with ethyl acetate and acidified with 2 mL 3 N HCl and ~8 mL 1 N HCl. The mixture was stirred to dissolve all the salts and filtered through celite. The layers were separated and the aqueous was extracted with ethyl acetate (total 150 mL). The combined organic layers were stirred with sodium sulfate and charcoal for 20 min. The mixture was then filtered through celite and concentrated in vacuo. MTBE (5 mL) was added to the residue and the mixture stirred. A solid formed and heptane (100 mL) was added and the mixture triturated for 15 h. The solid was collected by filtration, washed with heptane, and dried in vacuo to provide **27** (502 mg, 65%) as a yellow powder that was used without further purification. ^{1}H NMR (400 MHz, DMSO-d_6) δ 13.50 (br. s), 8.20 (d, J=8.6 Hz, 2H), 7.99 (d, J=8.6 Hz, 2H), 7.57 (s, 1H), 7.08 (s, 1H), 3.16 (s, 6H), 1.57 (s, 9H). LCMS calc. for $C_{19}H_{22}N_2O_4$ $(M+H)^+$: 343.2 found: 343.0.

*4-(4-(2'-(tert-Butyl)-7'-oxo-6',7'-dihydro-2'H-spiro[piperidine-4,5'-pyrano[3,2-c]pyrazole]-1-carbonyl)-6-(dimethylamino)pyridin-2-yl)benzoic acid (**10**).* Step 1: A vial was charged with **27** (50 mg, 0.15 mmol), **18** (48 mg, 0.16 mmol), HOBt (23 mg, 0.15 mmol), EDC (33 mg, 0.16 mmol), and dichloromethane (0.5 mL). Triethylamine (0.072 mL, 0.51 mmol) was added and the mixture stirred for 15 h. The mixture was diluted into ethyl acetate (15 mL) and washed with brine/water/1N HCl (1/1/0.1, 3 x 5 mL), saturated sodium bicarbonate solution (5 mL), brine (5 mL), dried over sodium sulfate, and concentrated in vacuo. The residue was purified by flash chromatography (20-50% ethyl acetate/heptane with 0.5% AcOH) to provide tert-butyl 4-(4-(2'-(tert-butyl)-7'-oxo-6',7'-dihydro-2'H-spiro[piperidine-4,5'-pyrano[3,2-c]pyrazole]-1-carbonyl)-6-(dimethylamino)pyridin-2-yl)benzoate (57 mg, 66%) as a pale yellow film. ^{1}H NMR (400 MHz, $CDCl_3$) δ 8.06 (s, 4H), 7.24 (s, 1H), 6.99 (d, *J*=0.6 Hz, 1H), 6.47 (d, *J*=0.8 Hz, 1H), 4.53 (br. d, *J*=13.1 Hz, 1H), 3.62 (d, *J*=12.3 Hz, 1H), 3.46 (br. t, *J*=13.1 Hz, 1H), 3.27 (br. t, *J*=13.1 Hz, 1H), 3.19 (s, 6H), 2.78–2.64 (m, 2H), 2.24 (br. d, *J*=14.0 Hz, 1H), 2.10 (s, 2H), 1.82–1.70 (m, 1H), 1.62 (s, 9H), 1.61 (s, 9H). LCMS calc. for $C_{33}H_{41}N_5O_5$ $(M+H)^+$: 588.3; found: 588.2.

Step 2: A round bottom flask was charged with tert-butyl 4-(4-(2'-(tert-butyl)-7'-oxo-6',7'-dihydro-2'H-spiro[piperidine-4,5'-pyrano[3,2-c]pyrazole]-1-carbonyl)-6-(dimethylamino)pyridin-2-yl)benzoate (57 mg, 0.097 mmol), dichloromethane (1.5 mL), and TFA (0.5 mL) and stirred at rt for 3 h. The mixture was diluted with dichloromethane and toluene and concentrated in vacuo. MeOH (2 x 10 mL) was then added and the mixture concentrated in vacuo. Minimal dichloromethane was then added followed by MTBE. The mixture was concentrated in vacuo to provide **10** (61 mg, quantitative). ^{1}H NMR (400 MHz, $CDCl_3$) δ 10.90 (br. s., 1H), 7.96 (d, *J*=8.0 Hz, 2H), 7.76 (d, *J*=7.8 Hz, 2H), 7.25 (s, *J*=6.7 Hz, 1H), 6.87 (s, 1H), 6.79 (s, 1H), 4.48 (br. d, *J*=11.9 Hz, 1H), 3.65–3.42 (m, 2H), 3.32 (s, 6H),

3.30–3.15 (m, 1H), 2.68 (s, 2H), 2.23 (br. d, *J*=12.9 Hz, 1H), 2.11 (br. d, *J*=13.5 Hz, 1H), 1.78–1.67 (m, 1H), 1.67–1.58 (m, 1H), 1.58 (s, 9H). LCMS calc. for $C_{29}H_{33}N_5O_5$ $(M+H)^+$: 532.3; found: 532.4.

*4-(6-(Dimethylamino)-4-(1-isopropyl-7-oxo-1,4,6,7-tetrahydrospiro[indazole-5,4'-piperidine]-1'-carbonyl)pyridin-2-yl)benzoic acid hydrochloride (**11**).* Step 1: 2,6-Dichloroisonicotinic acid (2.00 g, 10.42 mmol) was placed in a pressure tube and a solution of dimethylamine in tetrahydrofuran (26 mL, 2 M, 52 mmol) was added. The vessel was sealed and heated at 80 °C for 22 h. The mixture was cooled to room temperature, transferred to a round-bottom flask, and concentrated to dryness. The resulting white semi-solid was taken up in 30 mL of 0.1 M sodium hydroxide solution. 1 M HCl was added dropwise with stirring to adjust the pH of the solution to ca. 3.5, at which point a pale yellow solid formed. This was collected by filtration and dried under vacuum at 45 °C overnight to provide **26** inner salt (916 mg, 44 %). Further acidification of the aqueous solution to pH 1 resulted in the formation of a bright yellow solid, which was also collected and dried under vacuum to give **26**·HCl (1.15 g, 46%). For the HCl salt: ^{1}H NMR (400 MHz, DMSO-d_6) δ 13.64 (br. s, 1 H), 6.96 (d, *J*=1.0 Hz, 1 H), 6.89 (d, *J*=0.8 Hz, 1 H), 3.06 (s, 6 H), 2.53 (t, *J*=5.1 Hz, 1 H). LCMS calc. for $C_8H_9ClN_2O_2$ $(M+H)^+$: 201.0.; found: 201.1.

Step 2: A 20 mL microwave tube was charged with **26** (1.2 g, 5.1 mmol), 1,2-dimethoxyethane (10 mL), 4-tert-butyl ester phenylboronic acid (1.5 g, 6.8 mmol), aqueous Na_2CO_3 (2 M, 7 mL), and $PddppfCl_2 \cdot CH_2Cl_2$ (430 mg, 0.52 mmol). The reaction mixture was purged with nitrogen then sealed and heated to 100 °C in a microwave for 1.5 hours. The reaction was quenched with aqueous 1 M HCl and filtered through a pad of celite and washed with ethyl acetate. The layers were separated and the aqueous layer was extracted with ethyl acetate (x 2). The combined

organic layers were washed with brine, dried over Na_2SO_4, filtered, and concentrated in vacuo. The crude material was purified via silica gel chromatography once with 50–100% ethyl acetate/heptane and a second time using 0 to 10% MeOH/CH_2Cl_2. The resulting material showed a 50% mixture of starting material and product. This mixture was re-subjected to the reaction conditions by charging it to a 20 mL microwave tube along with 1,2-dimethoxyethane (10 mL), 4-tert-butyl ester phenylboronic acid (1.25 g, 5.6 mmol), aqueous Na_2CO_3 (2 M, 7 mL), and $PddppfCl_2 \cdot CH_2Cl_2$ (380 mg, 0.47 mmol) and heated to 120 °C in a microwave for 2 hours. The reaction was quenched with aqueous 1 M HCl and filtered through a pad of celite and washed with ethyl acetate. The layers were separated and the aqueous layer was extracted with ethyl acetate (x 2). The combined organic layers were washed with brine, dried over Na_2SO_4, filtered, and concentrated in vacuo. The crude material was purified via flash column chromatography (0-100% ethyl acetate/heptane) to provide **27** (1.6 g, ~75% purity) as a solid that was taken forward without further purification. ^{1}H NMR (400 MHz, DMSO-d_6) δ 13.50 (s, 1H), 8.23–8.17 (m, 2H), 8.02–7.95 (m, 2H), 7.57 (d, J = 0.6 Hz, 1H), 7.08 (d, J = 0.8 Hz, 1H), 3.16 (s, 6H). LCMS calc. for C19H22N2O4 $(M-H)^-$: 341.2; found: 341.0.

Step 3: To a solution of the **27** (1.09 g, 75% purity) in CH_2Cl_2 (20 mL) was added EDC (700 mg, 3.47 mmol) and HOBT (470 mg, 3.47 mmol). The reaction was stirred for 45 min before the addition of **28** dihydrochloride (820 mg, 2.56 mmol) and Hünig's base (2.0 mL, 12 mmol). The reaction was stirred for 16 h at rt. The reaction was quenched with saturated aqueous sodium bicarbonate solution and extracted with CH_2Cl_2 (x 2). The combined organic layers were washed with brine, dried over $MgSO_4$, filtered, and concentrated in vacuo. The crude material was purified via flash chromatography (0-100% ethyl acetate/heptane) to provide tert-butyl 4-(6-(dimethylamino)-4-(1-isopropyl-7-oxo-1,4,6,7-tetrahydrospiro[indazole-5,4'-piperidine]-1'-

carbonyl)pyridin-2-yl)benzoate (1.01 g, 48% over two steps) as a solid that was taken forward without further purification. ^{1}H NMR (400 MHz, $CDCl_3$) δ 8.10–8.00 (m, 4H), 7.40–7.39 (m, 1H), 7.00 (s, 1H), 6.56 (s, 1H), 5.38 (spt, *J* = 6.7 Hz, 1H), 3.89–3.68 (m, 2H), 3.49–3.37 (m, 2H), 3.23 (s, 6H), 2.84–2.80 (m, 2H), 2.62–2.58 (m, 2H), 1.75–1.67 (m, 2H), 1.62 (s, 9H), 1.58–1.50 (m, 2H), 1.50–1.42 (m, 6H). LCMS calc for $C_{33}H_{41}N_5O_4$ $(M+H)^+$: 572.3; found: 572.0.

Step 4: To a solution of tert-butyl 4-(6-(dimethylamino)-4-(1-isopropyl-7-oxo-1,4,6,7-tetrahydrospiro[indazole-5,4'-piperidine]-1'-carbonyl)pyridin-2-yl)benzoate (1.18 g, 2.06 mmol) in CH_2Cl_2 was added HCl in dioxane (4 M, 11 mL, 44 mmol). The reaction was stirred at rt for 30 min then concentrated in vacuo. NMR indicated that the reaction was not complete and the mixture was re-subjected to the above conditions. MeOH (10 mL) was added and the mixture was stirred for 30 min and concentrated in vacuo for 30 min. The material was purified using flash column chromatography (0-100% EtOAc/heptane then 0-20% MeOH/CH_2Cl_2). 100 mg of this material was dissolved in hot isopropanol (2 mL), cooled to rt, and stirred for 18 h to produce 60 mg of crystalline **11**. The remaining material was dissolved in 12 mL hot isopropanol, seeded, and cooled to rt, and stirred for 18 h. The resulting solid was collected via filtration, washed with 1.5 mL of cold isopropanol, and dried to produce **11** (580 mg, 55%) as the crystalline free form. ^{1}H NMR (400 MHz, CD_3OD) δ 8.18–8.14 (m, 2H), 8.11–8.07 (m, 2H), 7.42 (s, 1H), 7.12 (d, *J* = 0.8 Hz, 1H), 6.58 (d, *J* = 0.8 Hz, 1H), 5.38 (spt, *J* = 6.7 Hz, 1H), 3.95–3.82 (m, 1H), 3.76–3.65 (m, 1H), 3.51–3.45 (m, 2H), 3.19 (s, 6H), 2.89 (br. s, 2H), 2.65 (d, *J* = 2.7 Hz, 2H), 1.75 – 1.66 (m, 2H), 1.62 – 1.52 (m, 2H), 1.45 – 1.38 (m, 6H). LCMS calc. for $C_{29}H_{33}N_5O_4$ $(M+H)^+$: 516.3; found: 516.0.

*4-(4-(1-Isopropyl-7-oxo-1,4,6,7-tetrahydrospiro[indazole-5,4'-piperidine]-1'-carbonyl)-6-methoxypyridin-2-yl)benzoic acid (**12**).* Step 1: A round bottom flask was charged with **23** (202 g, 0.613 mol) and THF (700 mL). CDI (104.4 g, 0.644 mol) was then added and the reaction stirred at 72 °C for 1.5 h. The reaction mixture was cooled to 30 °C and triethylamine (202 mL, 1.45 mol) and **28** dihydrochloride (206 g, 0.643 mol) were added. Dichloromethane (900 mL) was then added to increase solubility of the reaction components. The reaction was then heated to 50 °C for 15 h. The reaction mixture was cooled to 20 °C and ethyl acetate (2.0 L) and 1 M NaOH (1.0 L) were added. The layers were separated and the organic layer was washed with 1 M HCl (2.0 L), brine, dried over sodium sulfate, filtered, and concentrated in vacuo. Flash column chromatography (ethyl acetate:petroleum ether, 1:2) was used to provide tert-butyl 4-(4-(1-isopropyl-7-oxo-1,4,6,7-tetrahydrospiro[indazole-5,4'-piperidine]-1'-carbonyl)-6-methoxypyridin-2-yl)benzoate (280 g, 81%) as a yellow solid. ^{1}H NMR (400 MHz, $CDCl_3$) δ 8.07 (s, 4H), 7.38 (s, 1H), 7.35 (d, *J*=0.8 Hz, 1H), 6.67 (d, *J*=0.8 Hz, 1H), 5.38 (spt, *J*=6.6 Hz, 1H), 4.06 (s, 3H), 3.84–3.69 (m, 2H), 3.46–3.36 (m, 2H), 2.88–2.75 (m, 2H), 2.65–2.55 (m, 2H), 1.75–1.67 (m, 2H), 1.62 (s, 9H), 1.58–1.51 (m, 2H), 1.50–1.38 (m, 6H). LCMS calc. for $C_{32}H_{38}N_4O_5$ $(M+H)^+$: 559.3; found: 559.1.

Step 2: A round bottomed flask was charged with tert-butyl 4-(4-(1-isopropyl-7-oxo-1,4,6,7-tetrahydrospiro[indazole-5,4'-piperidine]-1'-carbonyl)-6-methoxypyridin-2-yl)benzoate (280 g, 0.50 mol) and toluene (2.0 L). Phosphoric acid (85%, 240 mL) was added dropwise at 20 °C and the reaction was heated to 50 °C and stirred for 8 h. The reaction was cooled to rt and ethyl acetate (6.0 L) was added. The mixture was basified to pH 11 with 10% NaOH. The layers were separated and the organic layer set aside. The aqueous layer was acidified to pH 3-4 with 1 M HCl and extracted with ethyl acetate (3.0 L x 3). The combined organic layers were dried over

sodium sulfate, filtered, and concentrated in vacuo. The residue was dissolved in ethyl acetate (6.0 L) at 50 °C and petroleum ether (6.0 L) was added. The mixture was slowly cooled to rt and stirred for 16 h. The solids were collected via filtration and dried in vacuo. The solids were then treated with dichloromethane (8.0 L) and stirred at rt for 30 min. The mixture was filtered and the filtrate was concentrated in vacuo. Ethyl acetate was added to the mixture for co-evaporation and concentrated in vacuo to provide **12** (131.4 g, 52%) as a white solid. To further improve purity, this material was combined with a smaller batch of **12** (totaling 145.3 g, 289.1 mmol) in ethanol (1.45 L) and water (1.45 L) and heated to 45 °C for 48 h and cooled to rt. The mixture was stirred for 24 h at rt. The solids were collected by filtration, rinsed with ethanol/water (100 mL) and drive in vacuo at 50 °C for 16 h to provide **12** (144.8 g, quant.) as a white solid. ^{1}H NMR (600 MHz, DMSO-d_6) δ 13.05 (br. s, 1H), 8.25 (d, *J*=8.2 Hz, 2H), 8.04 (d, *J*=8.2 Hz, 2H), 7.63 (s, 1H), 7.45 (s, 1H), 6.81 (s, 1H), 5.26 (spt, *J*=6.5 Hz, 1H), 4.00 (s, 3H), 3.75–3.67 (m, 1H), 3.62–3.53 (m, 1H), 3.32-3.25 (m, 2H), 2.85–2.73 (m, 2H), 2.67–2.57 (m, 2H), 1.61–1.52 (m, 2H), 1.52–1.43 (m, 2H), 1.36 (d, *J*=6.5 Hz, 3H), 1.34 (d, *J*=6.5 Hz, 3H).

*4-(4-(1-Isopropyl-7-oxo-1,4,6,7-tetrahydrospiro[indazole-5,4'-piperidine]-1'-carbonyl)-6-methoxypyridin-2-yl)benzoic acid / 2-Amino-2-(hydroxymethyl)propane-1,3-diol salt (**12**·Tris).* A round bottomed flask fit with a mechanical stirred was charged with **12** (87.9 g, 175 mmol) and ethanol (1.2 L) and heated to 60 °C with stirring for 15 min to obtain a solution. Tris(2-aminoethyl)amine (23.5 g, 192 mmol) was then added and the mixture was stirred until a clear solution was obtained. Heptane (1 L) was added at 60 °C and the mixture was cooled to rt and stirred for 72 h. (Note, during this time, the mixture was re-heated to 45 °C for 3 h to produce a free-flowing slurry, which was then cooled to rt and stirred for 40 h at rt Two smaller batches of a similarly formed tris salt of **12** (11.29 g, 15.02 g) were added to form one uniform batch at this

step after stirring for 20 min. The mixture was filtered and rinsed with the mother liquor (30 mL) and dried in vacuo at 65 °C for 24 h to provide anhydrous **12**·Tris (128 g, 93%). ^{1}H NMR (600 MHz, DMSO-d_6) δ 8.12 (d, *J*=7.9 Hz, 2H), 7.99 (d, *J*=7.9 Hz, 2H), 7.56 (s, 1H), 7.45 (s, 1H), 7.30–5.64 (br. s, 6H), 6.75 (s, 1H), 5.27 (spt, *J*=6.5 Hz, 1H), 3.99 (s, 3H), 3.75–3.66 (m, 1H), 3.61–3.53 (m, 1H), 3.46 (s, 6H), 3.33–3.27 (m, 2H), 2.86–2.75 (m, 2H), 2.62 (s, 2H), 1.61–1.43 (m, 4H), 1.36 (d, *J*=6.7 Hz, 3H), 1.34 (d, *J*=6.7 Hz, 3H). HPLC purity: 99.2%.

Transport Studies in Transfected Human Embryonic Kidney 293 Cells. OATP1B1, OATP1B3, OATP2B1 or NTCP specific transport was assessed in stably transfected HEK 293 cells. Transporter-transfected and wild-type HEK293 cells were seeded onto 24-, 48-, or 98-well poly-D-lysine-coated cells at a density of 2 x 10^5 cells (24-well plate) per well in a total volume of 0.5 mL/well, 1.125 x 10^5 cells (48-well plate) per well in a total volume of 0.25 mL/well, or 2.5-5 x 10^4 cells/well in a total volume of 0.1 mL/well (96-well plate). OATP-transfected cells were cultured for 40–72 h in the presence of Dulbecco's modified Eagle's medium, 10% heat-inactivated FBS, and 5 μg/mL blasticidin. After the cells reached confluency, they were washed two times with uptake buffer (HBSS with 20 mM 4-(2-hydroxyethyl)-1-piperazineethanesulfonic acid, pH 7.4). The transport study was initiated by incubating the cells with incubation buffer containing each test compound at 37 °C. At the completion of the incubation (0.5–4.0 min), cells were quickly washed three times with ice-cold buffer. The cells were then lysed with MeOH containing an internal standard for analysis by liquid chromatography tandem mass spectrometry (LC-MS/MS). The uptake of test compounds was normalized by total cell protein using the BCA Protein Assay Kit following the manufacturer's protocol.

Transport Studies in Sandwich-Cultured Human Hepatocytes. Plateable cryopreserved hepatocytes were thawed and plated as described previously.[53] Briefly, hepatocytes were thawed

in a water bath at 37 °C and placed on ice. The cells were then poured into In VitroGro-HT medium at 37 °C at a ratio of one vial/50 mL in a conical tube. The cells were centrifuged at 50 x g for 3 min and resuspended at 0.75×10^6 cells/mL in In VitroGro-CP medium. Cell viability was determined by trypan blue exclusion and exceeded 85%. On day 1, hepatocyte suspensions were plated in collagen-coated 24-well plates at a density of 0.375×10^6 cells/well in a volume of 0.5 mL/well. After 18–24 h of incubation at 37 °C, cells were overlaid with ice-cold 0.25 mg/mL Matrigel in In VitroGro-HI medium at 0.5 mL/well. Cultures were maintained in In VitroGro-HI medium that was refreshed every 24 h. On day 5, the sandwich-cultured human hepatocytes were first rinsed twice with HBSS containing Ca^{2+}/Mg^{2+} (standard) or Ca^{2+}/Mg^{2+}-free HBSS, and then preincubated for 10 min with standard or Ca^{2+}/Mg^{2+}-free HBSS in the absence or presence of rifamycin SV (0.1 mM) at 37 °C. After aspirating the preincubation buffer, 0.5 mL of incubation buffer containing **12** (1 μM) was added in the absence or presence of rifamycin (0.1 mM) at 37 °C. The uptake was terminated at designated times (0–15 min) by adding 0.5 mL of ice-cold standard HBSS after removal of the incubation buffer. Cells were then washed three times with 0.5 mL of ice-cold standard HBSS. The hepatocytes were lysed with MeOH containing the internal standard for LC-MS/MS quantitation of **12**.

Animal Pharmacokinetic Studies. All experiments involving animals were conducted in our American Animal Association Laboratory Animal Care (AAALAC)-accredited facilities and were reviewed and approved by Pfizer Institutional Animal Care and Use Committee. Male Wistar-Hannover rats (weighing 240–350 g) underwent jugular vein cannulation (JVC) surgery at BioDuro, or in-house at Pfizer Inc., (Groton, CT); carotid artery cannula (CAC) / JVC rats were purchased from Taconic Biosciences (Hudson, NY). Rats were housed one per cage in an AAALAC accredited facility and maintained under standard conditions of temperature (22 °C ±

2 °C), relative humidity (50%) and light and dark cycle (12/12 h). Rats were allowed to acclimate to their environment for 1 week. In-life and bioanalytical studies were conducted at BioDuro (Beijing, China) or in-house (Pfizer Inc., Groton, CT). Rats received either a 1 mg/kg IV dose delivered by a volume of 2 mL/kg or a 5 mg/kg PO dose delivered by a volume of 5 mL/kg. Blood samples were collected in K2EDTA-treated tubes at the following time-points after dosing, 0.083, 0.25, 0.5, 1, 2, 4, 7, 24 h via tail vein bleed or by carotid artery cannula. Urine samples (4.0-7,0, and 7.0–24 h) were also collected after IV administration to rats. An IV dose of **12** (1 mg/kg) was also administered to bile duct-cannulated rats (n = 3), where bile samples were collected periodically on ice from 0–24 h and stored at – 20 °C until analysis. Blood samples were immediately centrifuged for plasma collection and stored at –80 °C prior to analysis of the parent compounds by LC-MS/MS. Aliquots of bile, or urine (20 μL) were transferred to 96-well blocks and acetonitrile (200 μL) containing an internal standard was added to each well, prior to analysis of **12** by LC-MS/MS. Rat liver exposure studies were conducted in male Wistar-Hannover rats following a single PO administration of **8** at 30 mg/kg or **11** at 10 mg/kg and **12** at 10 mg/kg. Blood and liver tissue samples were collected at 6 h post-dose and stored on ice until centrifugation. Blood samples were centrifuged to obtain plasma. The plasma and liver samples were stored at –80 °C prior to analysis of test compounds by LC-MS/MS.

Pharmacokinetic studies in male cynomolgus monkeys (weighing 6–11 kg) were conducted at Pfizer Inc., (Groton, CT). Monkeys were housed in an AAALAC accredited facility. For compound **12**, monkeys (n = 2) received either a 1 mg/kg IV dose delivered by a volume of 0.25 mL/kg in 2% NMP + 98% SBECD (12.5%) in 50 mM TRIS buffer, pH 8.0 or a 5 mg/kg PO dose delivered by a volume of 2 mL/kg as a suspension in 0.5% MC/0.1% tween80. Blood samples were collected via femoral vein into a syringe then transferred into K2EDTA-treated

vacutainer tubes at the following time-points after dosing, 0.083, 0.25, 0.5, 1, 2, 4, 7, 24, 32, 48, 56, and 72 h (IV) and 0.25, 0.5, 1, 2, 4, 7, 24 h (PO). Blood samples were centrifuged to obtain plasma and stored at –80 °C prior to analysis of **12** by LC-MS/MS. For determination of in vivo $Kp_{u,u}$, compound **12** (1 mg/kg) was also dosed IV as a solution in 2% NMP + 98% SBECD (12.5%) in 50 mM TRIS buffer, pH 8.0 to male cynomolgus monkeys (n = 2) at a dose volume of 0.25 mL/kg via the saphenous vein. Six hours post-dose, monkeys were euthanized, and terminal blood and liver (3 different 1-gram pieces from separate lobes/animal) samples were collected from each animal. Liver samples were rinsed with saline and patted dry with a paper towel, and all the blood vessels attached were also removed to minimize the potential contamination from blood and bile, then snap-frozen in liquid nitrogen and stored frozen until analysis. Blood samples were centrifuged to generate plasma which was then stored frozen until analysis. Liver samples were homogenized before sample extraction. Concentrations of **12** in plasma and liver were determined using LC-MS/MS. Free concentrations were calculated by multiplying the total plasma or total liver concentration by the f_u values of **12** in plasma or liver. The in vivo $K_{pu,u}$ was obtained by dividing the unbound liver concentration by the unbound plasma concentration.

Thermodynamic Solubility Measurement. Dry crystalline powders were pre-weighed into Whatman® Mini-Uniprep® syringeless filter devices with 0.45 pm polytetrafluoroethylene (PTFE) membranes. The desired medium (450 µL) was added to the filter vial and agitated for 24 hours at ambient temperature. After 24 hours, the sample was filtered and the filtrates were injected into the nitrogen detector for quantification on Analiza's Automated Discovery Workstation.™

Evaluation of DNL in Rats Treated with 12. Male Sprague-Dawley rats (weight ~200 g) were housed under standard laboratory conditions and kept under a reverse 12:12 h light-dark schedule. Rats were fed a standard laboratory rodent chow diet (5053 from LabDiet, Quakertown, PA). On the day of the experiment, rats were weighed, dosed PO (10 mL/kg) with a single administration of either vehicle control (0.5% methyl cellulose) or **12** at 0.03, 0.1, 0.3, 1, 3, 10, 30, 100 or 300 mg/kg. One hour post dose, rats were dosed by intraperitoneal injection with [^{14}C]-acetate (NEC553001MC from Perkin Elmer, Waltham, MA) at 0.1 μCi/g body weight. One hour post acetate dose, rats were euthanized by CO_2 asphyxiation. Blood was collected via cardiac puncture and centrifuged to obtain plasma for determination of plasma concentration of **12**. Samples from the right medial lobe of the liver, the right lung and bone marrow from the right femur were also collected and weighed. The procedure employed for tissue lipid extraction was previously published.[2] Non-linear fit was employed to determine the values for ED_{50} using GraphPad Prism.

Evaluation of Liver TG's in Rats Treated with 12. Male Sprague-Dawley rats (n = 40, ~200 g) were housed under standard laboratory conditions and kept under a reverse 12:12 h light-dark schedule. Rats were randomized into either chow (5053 from LabDiet, Quakertown, PA) or high-fat (D09032303Mi from Research Diets, New Brunswick, NJ) diet groups and were given a 18-day lead-in period on either diet prior to the start of the study. On day 1 of the study, rats were dosed PO once daily (10 mL/kg) with either vehicle control (0.25% methylcellulose) or **12** (tris salt) at 1, 3 or 10 mg/kg for 42 days. Rats were weighed twice weekly throughout the study and dosing volumes were adjusted accordingly. On the last day of the study (day 42), rats were dosed PO with **12** (1, 3 or 10 mg/kg) or vehicle. Two hours post dose, animals were euthanized by CO_2 asphyxiation. Livers were rapidly removed, freeze-clamped in a Wollenberg clamp pre-cooled in

liquid nitrogen then rapidly pulverized on an aluminum block pre-cooled in liquid nitrogen. To determine hepatic TG accumulation, approximately 50 mg of pulverized tissue was added to a 2 mL lysing matrix D tube (MP Bio, Irvine, CA) containing homogenization buffer, with a final ratio of 1:20 (w:v), tissue to homogenization buffer (10 mM TRIS pH 7.4, 0.9% NaCl and 0.2% Triton X100). Samples were immediately extracted, vortexed and then analyzed on a Siemens Chemistry XPT clinical analyzer (Malvern, PA).

Evaluation of DNL in NHPs Treated with 12. Twelve male cynomolgus macaques (age 6-14 years, weight ~ 7.5-12.5 kg) were used in a cross-over fashion. DNL was measured for each animal following PO administration of vehicle (0.5% MC) and **12** (10 mg/kg). A minimum of 14 days was allowed for washout between DNL determinations. Monkeys remained in their home cage for the majority of the study and were briefly chaired for PO gavage of test article and blood collection. In compliance with Institutional Animal Care and Use Committee fasting guidelines, each animal received a banana at the 2- and 3-hour time points. Food was restored immediately following completion of the study. On the day prior to the study, all 12 animals received a loading dose of deuterium oxide (D_2O, 151882 from Sigma-Aldrich, St. Louis, MO) at a volume of approximately 2.5% of their body water via PO gavage. Ad lib access to drinking water enriched to 5% D_2O was provided following the loading dose and animals were fasted overnight. Pre-dose blood samples were obtained and vehicle (0.5% w/v methylcellulose in 5% D_2O) or compound **12** (10 mg/kg) was administered via PO gavage. This was immediately followed by 10 mL 5% D_2O to ensure complete gastric delivery. A palatable solution of Prang (F2351 from Bioserve, Flemington, NJ) prepared in 5% D_2O, containing 0.83 g/mL fructose was used to deliver 5 g of fructose per time point. After administration of vehicle or **12**, the Prang solution was administered orally every 30 min starting at time t = 0 and continuing through the

8-hour time point. The monkeys had previously been conditioned to drink the fructose solution voluntarily while in their home cage. Blood samples (approximately 1 mL) were collected from each animal on the day of the study prior to vehicle or compound administration and at 2, 3, 4, 5, 6, 7, 8 and 9 hours post administration.

Plasma D_2O concentration was measured by Metabolic Solutions, Inc (Nashua, NH). Deuterium enrichment of plasma palmitate was measured using gas chromatography mass spectrometry (GC/MS). Plasma lipids were extracted by the method of Bligh and Dyer,[54] followed by transesterification to fatty acid methyl esters with boron trifluoride/MeOH, using the method of Morrison and Smith.[55] Fatty acid methyl esters (FAME) were analyzed by GC/MS using an Agilent 6890 GC coupled to an Agilent 5973 MS detector (Santa Clara, CA). FAME species were separated on an Agilent HP-5MS GC column (30 m, 0.25 mm, 0.25 μm). The GC method utilized a thermal gradient. FAME species were then analyzed on the MS detector using electron impact in the selected ion monitoring mode. GC chromatogram peak integration was performed with Agilent MassHunter software (Santa Clara, CA).

NHP Safety Studies with 12. Male and female Mauritius origin cynomolgus monkeys (*Macaca fascicularis*) approximately 3-5 years of age at dose initiation were cared for in accordance with the Guide for the Care and Use of Laboratory Animals (Institute for Laboratory Animal Resources publication, 1996, NRC Press, Ottawa, Canada). Animals were housed at an indoor, Association for Assessment and Accreditation of Laboratory Animal Care International–accredited facility in species-specific housing. All experimental study protocols involving animals used in these studies and their housing conditions were reviewed and approved by Pfizer Institutional Animal Care and Use Committee. Certified Primate Diet (PMI Feeds 5K91; Richmond, IN) was provided daily in amounts appropriate for the age and size of the animals.

Municipal drinking water, further purified by reverse osmosis, was available ad libitum to each animal via an automatic watering system. The animals were given additional supplements as a form of environmental enrichment and were given various cage-enrichment devices. Animals were maintained on a 12:12 h light:dark cycle in rooms at 66 ºF to 77 ºF and relative humidity of 30% to 70%.

Male (n = 3/group) and female (n = 3/group) cynomolgus monkeys were administered **12** (in 0.25% methylcellulose) once daily by PO gavage at 3, 10, 30, or 90 mg/kg/day for 14 days. A concurrent control group received the vehicle by the same route and regimen. Animals were evaluated for clinical signs, body weight, food consumption, clinical pathology parameters (prior to the initiation of dosing and at necropsy), and determination of plasma concentrations of **12**. Following the administration of the last dose, animals were sedated, euthanized by exsanguination, and necropsied. Organ weights were collected and a full set of tissues was examined microscopically by a board-certified veterinary pathologist.

ASSOCIATED CONTENT

Supporting Information.

The following files are available free of charge.

Molecular formula strings (CSV)

AUTHOR INFORMATION

Corresponding Author

*E-mail: Aaron.Smith2@Pfizer.com

Author Contributions

All authors have given approval to the final version of the manuscript.

Notes

The authors declare the following competing interest(s): All authors were employed by Pfizer for the duration of the work described in the manuscript. All procedures performed on animals were in accordance with regulations and established guidelines and were reviewed and approved by the Pfizer Institutional Animal Care and Use Committee.

ACKNOWLEDGMENT

The authors would like to thank Thomas V. Magee and Daniel W. Kung for scientific discussions, contributions to the work reported here, and manuscript revisions.

ABBREVIATIONS

ACC, acetyl-Coa carboxylase; AUC, area under the plasma concentration-time curve; Boc, *t*-butyloxycarbonyl; CDI, carbonyldiimidazole; CL_p, plasma clearance; CL_{active}, hepatic uptake clearance; $CL_{int,met}$, metabolic intrinsic clearance; C_{max}, maximal plasma concentration; $CL_{passive}$, passive clearance; CYP450, cytochrome P450; DMAc, *N,N*-dimethylacetamide; DMF, *N,N*-dimethylformamide; DMSO, dimethyl sulfoxide; DNL, de novo lipogenesis; EDC, *N*-(3-Dimethylaminopropyl)-*N*′-ethylcarbodiimide hydrochloride; F, oral bioavailability; FAME, fatty acid methyl esters; f_u, unbound fraction in plasma or liver; GC/MS, gas chromatography mass spectrometry; h, hours; HATU, *N*-[(Dimethylamino)-1*H*-1,2,3-triazolo-[4,5-b]pyridin-1-ylmethylene]-*N*-methylmethanaminium hexafluorophosphate *N*-oxide; hERG, human Ether-à-go-go; HHEP, human hepatocytes; HOBT, 1-Hydroxybenzotriazole hydrate; HPLC, high performance liquid chromatography; IV, intravenous administration; $K_{pu,u}$, unbound liver-to-plasma ratio; LCMS, liquid chromatography mass spectrometry; LC-MS/MS, liquid

chromatography tandem mass spectrometry; MC, methyl cellulose; min, minutes; NAFLD, non-alcoholic fatty liver disease; NASH, non-alcoholic steatohepatitis; NBS, *N*-bromosuccinimide; NHP, nonhuman primate; NMM, *N*-methylmorpholine; NTCP, sodium-taurocholate cotransporting polypeptide; OATP, organic anion transporting polypeptide; Oatp, rodent organic anion transporting polypeptide; P_{app}, permeability; PO, oral administration; $t_{1/2}$, half-life; T2DM, type 2 diabetes mellitus; TFA, trifluoroacetic acid; TG, triglycerides; T_{max}, time of first occurrence of C_{max}; Tris, 2-Amino-2-(hydroxymethyl)propane-1,3-diol; UHP, urea-hydrogen peroxide; V_{ss}, steady state volume of distribution.

REFERENCES

1. Saggerson, D. Malonyl-CoA, a Key Signaling Molecule in Mammalian Cells. *Annu. Rev. Nutr.* **2008,** 28, 253-272.
2. Harwood, H. J., Jr.; Petras, S. F.; Shelly, L. D.; Zaccaro, L. M.; Perry, D. A.; Makowski, M. R.; Hargrove, D. M.; Martin, K. A.; Tracey, W. R.; Chapman, J. G.; Magee, W. P.; Dalvie, D. K.; Soliman, V. F.; Martin, W. H.; Mularski, C. J.; Eisenbeis, S. A. Isozyme-Nonselective N-Substituted Bipiperidylcarboxamide Acetyl-CoA Carboxylase Inhibitors Reduce Tissue Malonyl-CoA Concentrations, Inhibit Fatty Acid Synthesis, and Increase Fatty Acid Oxidation in Cultured Cells and in Experimental Animals. *J. Biol. Chem.* **2003,** 278, 37099-37111.
3. Alkhouri, N.; Lawitz, E.; Noureddin, M.; DeFronzo, R.; Shulman, G. I. GS-0976 (Firsocostat): An Investigational Liver-Directed Acetyl-CoA Carboxylase (ACC) Inhibitor for the Treatment of Non-Alcoholic Steatohepatitis (NASH). *Expert Opin. Investig. Drugs* **2020,** 29, 135-141.
4. Kim, C. W.; Addy, C.; Kusunoki, J.; Anderson, N. N.; Deja, S.; Fu, X.; Burgess, S. C.; Li, C.; Ruddy, M.; Chakravarthy, M.; Previs, S.; Milstein, S.; Fitzgerald, K.; Kelley, D. E.; Horton, J. D. Acetyl CoA Carboxylase Inhibition Reduces Hepatic Steatosis but Elevates Plasma Triglycerides in Mice and Humans: A Bedside to Bench Investigation. *Cell Metab.* **2017,** 26, 394-406.e396.
5. Harriman, G.; Greenwood, J.; Bhat, S.; Huang, X.; Wang, R.; Paul, D.; Tong, L.; Saha, A. K.; Westlin, W. F.; Kapeller, R.; Harwood, H. J. Acetyl-CoA Carboxylase Inhibition by ND-630 Reduces Hepatic Steatosis, Improves Insulin Sensitivity, and Modulates Dyslipidemia in Rats. *Proc. Natl. Acad. Sci.* **2016,** 113, E1796-E1805. Note that compound **12** was originally disclosed in 2012 (see ref. 28).
6. Stiede, K.; Miao, W.; Blanchette, H. S.; Beysen, C.; Harriman, G.; Harwood, H. J.; Kelley, H.; Kapeller, R.; Schmalbach, T.; Westlin, W. F. Acetyl-Coenzyme a Carboxylase Inhibition Reduces De Novo Lipogenesis in Overweight Male Subjects: A Randomized, Double-Blind, Crossover Study. *Hepatology* **2017,** 66, 324-334.

7. Jones, J. E.; Esler, W. P.; Patel, R.; Lanba, A.; Vera, N. B.; Pfefferkorn, J. A.; Vernochet, C. Inhibition of Acetyl-CoA Carboxylase 1 (ACC1) and 2 (ACC2) Reduces Proliferation and De Novo Lipogenesis of EGFRvIII Human Glioblastoma Cells. *PLoS One* **2017,** 12, e0169566.
8. Lally, J. S. V.; Ghoshal, S.; DePeralta, D. K.; Moaven, O.; Wei, L.; Masia, R.; Erstad, D. J.; Fujiwara, N.; Leong, V.; Houde, V. P.; Anagnostopoulos, A. E.; Wang, A.; Broadfield, L. A.; Ford, R. J.; Foster, R. A.; Bates, J.; Sun, H.; Wang, T.; Liu, H.; Ray, A. S.; Saha, A. K.; Greenwood, J.; Bhat, S.; Harriman, G.; Miao, W.; Rocnik, J. L.; Westlin, W. F.; Muti, P.; Tsakiridis, T.; Harwood, H. J.; Kapeller, R.; Hoshida, Y.; Tanabe, K. K.; Steinberg, G. R.; Fuchs, B. C. Inhibition of Acetyl-CoA Carboxylase by Phosphorylation or the Inhibitor ND-654 Suppresses Lipogenesis and Hepatocellular Carcinoma. *Cell Metab.* **2019,** 29, 174-182.e175.
9. Esler, W. P.; Tesz, G. J.; Hellerstein, M. K.; Beysen, C.; Sivamani, R.; Turner, S. M.; Watkins, S. M.; Amor, P. A.; Carvajal-Gonzalez, S.; Geoly, F. J.; Biddle, K. E.; Purkal, J. J.; Fitch, M.; Buckeridge, C.; Silvia, A. M.; Griffith, D. A.; Gorgoglione, M.; Hassoun, L.; Bosanac, S. S.; Vera, N. B.; Rolph, T. P.; Pfefferkorn, J. A.; Sonnenberg, G. E. Human Sebum Requires De Novo Lipogenesis, Which Is Increased in Acne Vulgaris and Suppressed by Acetyl-CoA Carboxylase Inhibition. *Sci. Transl. Med.* **2019,** 11, eaau8465.
10. Corbett, J. W.; Freeman-Cook, K. D.; Elliott, R.; Vajdos, F.; Rajamohan, F.; Kohls, D.; Marr, E.; Zhang, H.; Tong, L.; Tu, M.; Murdande, S.; Doran, S. D.; Houser, J. A.; Song, W.; Jones, C. J.; Coffey, S. B.; Buzon, L.; Minich, M. L.; Dirico, K. J.; Tapley, S.; McPherson, R. K.; Sugarman, E.; Harwood, H. J., Jr.; Esler, W. Discovery of Small Molecule Isozyme Non-Specific Inhibitors of Mammalian Acetyl-CoA Carboxylase 1 and 2. *Bioorg. Med. Chem. Lett.* **2010,** 20, 2383-2388.
11. Freeman-Cook, K. D.; Amor, P.; Bader, S.; Buzon, L. M.; Coffey, S. B.; Corbett, J. W.; Dirico, K. J.; Doran, S. D.; Elliott, R. L.; Esler, W.; Guzman-Perez, A.; Henegar, K. E.; Houser, J. A.; Jones, C. S.; Limberakis, C.; Loomis, K.; McPherson, K.; Murdande, S.; Nelson, K. L.; Phillion, D.; Pierce, B. S.; Song, W.; Sugarman, E.; Tapley, S.; Tu, M.; Zhao, Z. Maximizing Lipophilic Efficiency: The Use of Free-Wilson Analysis in the Design of Inhibitors of Acetyl-CoA Carboxylase. *J. Med. Chem.* **2012,** 55, 935-942.
12. Griffith, D. A.; Dow, R. L.; Huard, K.; Edmonds, D. J.; Bagley, S. W.; Polivkova, J.; Zeng, D.; Garcia-Irizarry, C. N.; Southers, J. A.; Esler, W.; Amor, P.; Loomis, K.; McPherson, K.; Bahnck, K. B.; Preville, C.; Banks, T.; Moore, D. E.; Mathiowetz, A. M.; Menhaji-Klotz, E.; Smith, A. C.; Doran, S. D.; Beebe, D. A.; Dunn, M. F. Spirolactam-Based Acetyl-CoA Carboxylase Inhibitors: Toward Improved Metabolic Stability of a Chromanone Lead Structure. *J. Med. Chem.* **2013,** 56, 7110-7119.
13. Griffith, D. A.; Kung, D. W.; Esler, W. P.; Amor, P. A.; Bagley, S. W.; Beysen, C.; Carvajal-Gonzalez, S.; Doran, S. D.; Limberakis, C.; Mathiowetz, A. M.; McPherson, K.; Price, D. A.; Ravussin, E.; Sonnenberg, G. E.; Southers, J. A.; Sweet, L. J.; Turner, S. M.; Vajdos, F. F. Decreasing the Rate of Metabolic Ketone Reduction in the Discovery of a Clinical Acetyl-CoA Carboxylase Inhibitor for the Treatment of Diabetes. *J. Med. Chem.* **2014,** 57, 10512-10526.
14. Kelley, K. L. R., W. J.; Sonnenberg, G. E.; Clasquin, M.; Amor, P. A.; Carvajal-Gonzalez, S.; Shirai, N.; Matthews, M. D.; Li, K. W.; Hellerstein, M. K.; Vera, N. B.; Ross, T. T.; Cappon, G.; Bergman, A.; Buckeridge, C.; Sun, Z.; Qejvanaj, E. Z.; Schmahai, T.; Beebe, D.; Pfefferkorn, J. A.; Esler, W. P. De Novo Lipogenesis Is Essential for Platelet Production in Humans. *Nat. Metab.* **2020**, Manuscript In Press.
15. Sumida, Y.; Yoneda, M. Current and Future Pharmacological Therapies for NAFLD/NASH. *J. Gastroenterol.* **2018,** 53, 362-376.

16. Romero, F. A.; Jones, C. T.; Xu, Y.; Fenaux, M.; Halcomb, R. L. The Race to Bash NASH: Emerging Targets and Drug Development in a Complex Liver Disease. *J. Med. Chem.* **2020,** 63, 5031–5073.
17. Sanyal, A. J.; Friedman, S. L.; McCullough, A. J.; Dimick-Santos, L.; American Association for the Study of Liver, D.; United States, F.; Drug, A. Challenges and Opportunities in Drug and Biomarker Development for Nonalcoholic Steatohepatitis: Findings and Recommendations from an American Association for the Study of Liver Diseases-U.S. Food and Drug Administration Joint Workshop. *Hepatology* **2015,** 61, 1392-1405.
18. Chalasani, N.; Younossi, Z.; Lavine, J. E.; Diehl, A. M.; Brunt, E. M.; Cusi, K.; Charlton, M.; Sanyal, A. J. The Diagnosis and Management of Non-Alcoholic Fatty Liver Disease: Practice Guideline by the American Association for the Study of Liver Diseases, American College of Gastroenterology, and the American Gastroenterological Association. *Hepatology* **2012,** 55, 2005-2023.
19. Schutz, Y. Concept of Fat Balance in Human Obesity Revisited with Particular Reference to De Novo Lipogenesis. *Int. J. Obes.* **2004,** 28, S3-S11.
20. Savage, D. B.; Choi, C. S.; Samuel, V. T.; Liu, Z. X.; Zhang, D.; Wang, A.; Zhang, X. M.; Cline, G. W.; Yu, X. X.; Geisler, J. G.; Bhanot, S.; Monia, B. P.; Shulman, G. I. Reversal of Diet-Induced Hepatic Steatosis and Hepatic Insulin Resistance by Antisense Oligonucleotide Inhibitors of Acetyl-CoA Carboxylases 1 and 2. *J. Clin. Invest.* **2006,** 116, 817-824.
21. Goedeke, L.; Bates, J.; Vatner, D. F.; Perry, R. J.; Wang, T.; Ramirez, R.; Li, L.; Ellis, M. W.; Zhang, D.; Wong, K. E.; Beysen, C.; Cline, G. W.; Ray, A. S.; Shulman, G. I. Acetyl-CoA Carboxylase Inhibition Reverses NAFLD and Hepatic Insulin Resistance but Promotes Hypertriglyceridemia in Rodents. *Hepatology* **2018,** 68, 2197-2211.
22. Lawitz, E. J.; Poordad, F.; Coste, A.; Loo, N.; Djedjos, C. S.; McColgan, B.; Jia, C.; Xu, R.; Myers, R. P.; Subramanian, G. M.; McHutchison, J. G.; Middleton, M. S.; Sirlin, C.; Nyangau, E.; Fitch, M.; Li, K.; Hellerstein, M. Acetyl-CoA Carboxylase (ACC) Inhibitor GS-0976 Leads to Suppression of Hepatic De Novo Lipogenesis and Significant Improvements in MRI-PDFF, MRE, and Markers of Fibrosis after 12 Weeks of Therapy in Patients with NASH. *J. Hepatol.* **2017,** 66, S34.
23. Loomba, R.; Kayali, Z.; Noureddin, M.; Ruane, P.; Lawitz, E. J.; Bennett, M.; Wang, L.; Harting, E.; Tarrant, J. M.; McColgan, B. J.; Chung, C.; Ray, A. S.; Subramanian, G. M.; Myers, R. P.; Middleton, M. S.; Lai, M.; Charlton, M.; Harrison, S. A. GS-0976 Reduces Hepatic Steatosis and Fibrosis Markers in Patients with Nonalcoholic Fatty Liver Disease. *Gastroenterology* **2018,** 155, 1463-1473.e1466.
24. Kupčová, V.; Fedelešová, M.; Bulas, J.; Kozmonová, P.; Turecký, L. Overview of the Pathogenesis, Genetic, and Non-Invasive Clinical, Biochemical, and Scoring Methods in the Assessment of NAFLD. *Int. J. Environ. Res. Public Health* **2019,** 16, 3570.
25. Roth, M.; Obaidat, A.; Hagenbuch, B. OATPs, OATs and OCTs: The Organic Anion and Cation Transporters of the SLCO and SLC22A Gene Superfamilies. *Br. J. Pharmacol.* **2012,** 165, 1260-1287.
26. Kalliokoski, A.; Niemi, M. Impact of OATP Transporters on Pharmacokinetics. *Br. J. Pharmacol.* **2009,** 158, 693-705.
27. Varma, M. V.; Steyn, S. J.; Allerton, C.; El-Kattan, A. F. Predicting Clearance Mechanism in Drug Discovery: Extended Clearance Classification System (ECCS). *Pharm. Res.* **2015,** 32, 3785-3802.

28. Didiuk, M. T.; Dow, R. L.; Griffith, D. A. Preparation of Pyrazolospiroketone Acetyl-CoA Carboxylase Inhibitors. WO2012042433A1, 2012.
29. Varma, M. V.; Chang, G.; Lai, Y.; Feng, B.; El-Kattan, A. F.; Litchfield, J.; Goosen, T. C. Physicochemical Property Space of Hepatobiliary Transport and Computational Models for Predicting Rat Biliary Excretion. *Drug Metab. Dispos.* **2012,** 40, 1527-1537.
30. Tu, M.; Mathiowetz, A. M.; Pfefferkorn, J. A.; Cameron, K. O.; Dow, R. L.; Litchfield, J.; Di, L.; Feng, B.; Liras, S. Medicinal Chemistry Design Principles for Liver Targeting through OATP Transporters. *Curr. Top. Med. Chem.* **2013,** 13, 857-866.
31. Powell, D. A.; Black, W. C.; Bleasby, K.; Chan, C. C.; Deschenes, D.; Gagnon, M.; Gordon, R.; Guay, J.; Guiral, S.; Hafey, M. J.; Huang, Z.; Isabel, E.; Leblanc, Y.; Styhler, A.; Xu, L. J.; Zhang, L.; Oballa, R. M. Nicotinic Acids: Liver-Targeted SCD Inhibitors with Preclinical Anti-Diabetic Efficacy. *Bioorg. Med. Chem. Lett.* **2011,** 21, 7281-7286.
32. Pfefferkorn, J. A. Strategies for the Design of Hepatoselective Glucokinase Activators to Treat Type 2 Diabetes. *Expert Opin. Drug Discov.* **2013,** 8, 319-330.
33. Hagenbuch, B.; Meier, P. J. Organic Anion Transporting Polypeptides of the OATP/ SLC21 Family: Phylogenetic Classification as OATP/ SLCO Superfamily, New Nomenclature and Molecular/Functional Properties. *Pflugers Arch.* **2004,** 447, 653-665.
34. Di, L.; Whitney-Pickett, C.; Umland, J. P.; Zhang, H.; Zhang, X.; Gebhard, D. F.; Lai, Y.; Federico, J. J., 3rd; Davidson, R. E.; Smith, R.; Reyner, E. L.; Lee, C.; Feng, B.; Rotter, C.; Varma, M. V.; Kempshall, S.; Fenner, K.; El-Kattan, A. F.; Liston, T. E.; Troutman, M. D. Development of a New Permeability Assay Using Low-Efflux MDCKII Cells. *J. Pharm. Sci.* **2011,** 100, 4974-4985.
35. Stopher, D.; McClean, S. An Improved Method for the Determination of Distribution Coefficients. *J. Pharm. Pharmacol.* **1990,** 42, 144.
36. Di, L.; Keefer, C.; Scott, D. O.; Strelevitz, T. J.; Chang, G.; Bi, Y.-A.; Lai, Y.; Duckworth, J.; Fenner, K.; Troutman, M. D.; Obach, R. S. Mechanistic Insights from Comparing Intrinsic Clearance Values between Human Liver Microsomes and Hepatocytes to Guide Drug Design. *Eur. J. Med. Chem.* **2012,** 57, 441-448.
37. Kimoto, E.; Vourvahis, M.; Scialis, R. J.; Eng, H.; Rodrigues, A. D.; Varma, M. V. S. Mechanistic Evaluation of the Complex Drug-Drug Interactions of Maraviroc: Contribution of Cytochrome P450 3A, P-Glycoprotein and Organic Anion Transporting Polypeptide 1B1. *Drug Metab. Dispos.* **2019,** 47, 493-503.
38. Tweedie, D.; Polli, J. W.; Berglund, E. G.; Huang, S. M.; Zhang, L.; Poirier, A.; Chu, X.; Feng, B.; International Transporter, C. Transporter Studies in Drug Development: Experience to Date and Follow-up on Decision Trees from the International Transporter Consortium. *Clin. Pharmacol. Ther.* **2013,** 94, 113-125.
39. Banker, M. J.; Clark, T. H.; Williams, J. A. Development and Validation of a 96-Well Equilibrium Dialysis Apparatus for Measuring Plasma Protein Binding. *J. Pharm. Sci.* **2003,** 92, 967-974.
40. Kalgutkar, A. S.; Frederick, K. S.; Hatch, H. L.; Ambler, C. M.; Perry, D. A.; Garigipati, R. S.; Chang, G. C.; Lefker, B. A.; Clark, R. W.; Morehouse, L. A.; Francone, O.; Hu, X. Identification of a Novel, Non-Tetrahydroquinoline Variant of the Cholesteryl Ester Transfer Protein (CETP) Inhibitor Torcetrapib, with Improved Aqueous Solubility. *Xenobiotica* **2014,** 44, 591-605.
41. Ross, T. T.; Crowley, C.; Kelly, K.; Rinaldi, A.; Beebe, D. A.; Lech, M. P.; Martinez, R. V.; Carvajal-Gonzalez, S.; Boucher, M.; Hirenallur-Shanthappa, D.; Morin, J.; Opsahl, A.;

Vargas, S. R.; Pfefferkorn, J. A.; Esler, W. P. Acetyl-CoA Carboxylase Inhibitor PF-05221304 Improves Multiple Dimensions of NASH Pathogenesis in Experimental Model Systems. *Cell. Mol. Gastroenterol. Hepatol.* **2020,** Manuscript in Press https://doi.org/10.1016/j.jcmgh.2020.06.001.

42. Kimoto, E.; Bi, Y.-A.; Kosa, R. E.; Tremaine, L. M.; Varma, M. V. S. Hepatobiliary Clearance Prediction: Species Scaling from Monkey, Dog, and Rat, and In vitro–In vivo Extrapolation of Sandwich-Cultured Human Hepatocytes Using 17 Drugs. *J. Pharm. Sci.* **2017,** 106, 2795-2804.

43. Di, L.; Atkinson, K.; Orozco, C. C.; Funk, C.; Zhang, H.; McDonald, T. S.; Tan, B.; Lin, J.; Chang, C.; Obach, R. S. In Vitro–in Vivo Correlation for Low-Clearance Compounds Using Hepatocyte Relay Method. *Drug Metab. Dispos.* **2013,** 41, 2018-2023.

44. Walsky, R. L.; Obach, R. S. Validated Assays for Human Cytochrome P450 Activities. *Drug Metab. Dispos.* **2004,** 32, 647.

45. Orr, S. T. M.; Ripp, S. L.; Ballard, T. E.; Henderson, J. L.; Scott, D. O.; Obach, R. S.; Sun, H.; Kalgutkar, A. S. Mechanism-Based Inactivation (MBI) of Cytochrome P450 Enzymes: Structure–Activity Relationships and Discovery Strategies to Mitigate Drug–Drug Interaction Risks. *J. Med. Chem.* **2012,** 55, 4896-4933.

46. Walsky, R. L.; Bauman, J. N.; Bourcier, K.; Giddens, G.; Lapham, K.; Negahban, A.; Ryder, T. F.; Obach, R. S.; Hyland, R.; Goosen, T. C. Optimized Assays for Human UDP-Glucuronosyltransferase (UGT) Activities: Altered Alamethicin Concentration and Utility to Screen for UGT Inhibitors. *Drug Metab. Dispos.* **2012,** 40, 1051-1065.

47. Lapham, K.; Novak, J.; Marroquin, L. D.; Swiss, R.; Qin, S.; Strock, C. J.; Scialis, R.; Aleo, M. D.; Schroeter, T.; Eng, H.; Rodrigues, A. D.; Kalgutkar, A. S. Inhibition of Hepatobiliary Transport Activity by the Antibacterial Agent Fusidic Acid: Insights into Factors Contributing to Conjugated Hyperbilirubinemia/Cholestasis. *Chem. Res. Toxicol.* **2016,** 29, 1778-1788.

48. Aleo, M. D.; Luo, Y.; Swiss, R.; Bonin, P. D.; Potter, D. M.; Will, Y. Human Drug-Induced Liver Injury Severity Is Highly Associated with Dual Inhibition of Liver Mitochondrial Function and Bile Salt Export Pump. *Hepatology* **2014,** 60, 1015-1022.

49. Beysen, C.; Ruddy, M.; Stoch, A.; Mixson, L.; Rosko, K.; Riiff, T.; Turner, S. M.; Hellerstein, M. K.; Murphy, E. J. Dose-Dependent Quantitative Effects of Acute Fructose Administration on Hepatic De Novo Lipogenesis in Healthy Humans. *Am. J. Physiol. Endocrinol. Metab.* **2018,** 315, E126-E132.

50. Bergman, A.; Gonzalez, S. C.; Tarabar, S.; Saxena, A.; Esler, W.; Amin, N. Safety, Tolerability, Pharmacokinetics and Pharmacodynamics of a Liver-Targeting ACC Inhibitor (PF-05221304) Following Single and Multiple Oral Doses. *J. Hepatol.* **2018,** 68, S582.

51. Bergman, A.; Carvajal-Gonzalez, S.; Tarabar, S.; Saxena, A. R.; Esler, W. P.; Amin, N. B. Safety, Tolerability, Pharmacokinetics, and Pharmacodynamics of a Liver-Targeting Acetyl-CoA Carboxylase Inhibitor (PF-05221304): A Three-Part Randomized Phase 1 Study. *Clin. Pharmacol. Drug Dev.* **2020,** 9, 514-526.

52. Bagley, S. W.; Southers, J. A.; Cabral, S.; Rose, C. R.; Bernhardson, D. J.; Edmonds, D. J.; Polivkova, J.; Yang, X.; Kung, D. W.; Griffith, D. A.; Bader, S. J. Synthesis of 7-Oxo-Dihydrospiro[Indazole-5,4′-Piperidine] Acetyl-CoA Carboxylase Inhibitors. *J. Org. Chem.* **2012,** 77, 1497-1506.

53. Kimoto, E.; Li, R.; Scialis, R. J.; Lai, Y.; Varma, M. V. S. Hepatic Disposition of Gemfibrozil and Its Major Metabolite Gemfibrozil 1-O-B-Glucuronide. *Mol. Pharm.* **2015,** 12, 3943-3952.
54. Bligh, E. G.; Dyer, W. J. A Rapid Method of Total Lipid Extraction and Purification. *Can. J. Biochem. Physiol.* **1959,** 37, 911-917.
55. Morrison, W. R.; Smith, L. M. Preparation of Fatty Acid Methyl Esters and Dimethylacetals from Lipids with Boron Fluoride--Methanol. *J. Lipid Res.* **1964,** 5, 600-608.

TABLE OF CONTENT GRAPHIC